Int. J. Heat Mass Transfer. Vol. 22, pp. 401–420

0017-9310/79/0301-0401 $02.00/0

GLOBAL NUMERICAL SOLUTIONS OF GROWTH AND DEPARTURE OF A VAPOUR BUBBLE AT A HORIZONTAL SUPERHEATED WALL IN A PURE LIQUID AND A BINARY MIXTURE

W. ZIJL,* F. J. M. RAMAKERS and S. J. D. VAN STRALEN
Eindhoven University of Technology, Laboratory for Fluid Dynamics and Heat Transfer, Eindhoven, The Netherlands

(*Received* 7 *November* 1977)

Abstract—The growth and buoyancy induced departure of vapour bubbles at a horizontal superheated wall has been studied by global numerical methods. Integral forms of the heat transport equation have been solved by use of series expansions, obtained by the theory of fractional derivatives. The global orthogonal collocation method has been applied for the potential flow around the bubble. In this way a set of only eight or ten ordinary differential equations has to be integrated by computer. The results, following from prescribed initial temperature distributions, are in quantitative agreement with experimental data, obtained in water and aqueous binary mixtures, boiling at subatmospheric pressures.

NOMENCLATURE

a, $= k/\rho c$, liquid thermal diffusivity [m^2/s], $= (\dot{R}_c/R_c)^2$ in equation (9) [$1/s^2$], expansion coefficient in series for velocity potential [m^{3+2k}/s];
A, surface of bubble cap [m^2];
b, $= -\ddot{R}_c$, deceleration of liquid in hydrodynamic boundary layer at $r = R_c$[m/s^2], expansion coefficient in series for bubble radius [m];
c, liquid specific heat at constant pressure [m^2/s^2 K], $= 2\sigma/\rho$ in equation (9) [m^3/s^2];
C, concentration of more volatile component A in liquid B [kg/m^3];
C_0, initial bubble growth rate [m/s];
D, diffusion coefficient for more volatile component A [m^2/s];
E_m, E_p, memory series in equation (19) [m^3/s^2];
f, $x = f$, real solution of $ax^3 + bx^2 - c = 0$, continuous in a, b, c [m], symbol for general function;
f_0, expression for f when $4b^3/27a^2c \leqslant 1$ [m];
f_∞, expression for f when $4b^3/27a^2c \geqslant 1$ [m];
g, gravitational acceleration [m/s^2];
G_m, G_p, memory series in equation (30) [m/s];
h, thickness of liquid layer, especially of microlayer [m];
h_0, thickness of formation at $r = R_c$ of liquid microlayer [m];
H, initial height of thermal boundary layer above superheated wall [m];
i, integer number denoting collocation angle;
j, integer number;
Ja, $= \rho c\theta_0/\rho_v l$ Jakob number;
k, liquid thermal conductivity [kgm/s^3 K], integer number in series expansion for velocity potential;
l, latent enthalpy of vaporization [m^2/s^2];
l_m, latent enthalpy of vaporization in gas–vapour mixture [m^2/s^2];
M_A, molar mass of more volatile component A [kg/kmol];
M_B, molar mass of liquid B and its vapour [kg/kmol];
$\mathbf{n}$, unit vector normal to vapour–liquid interface;
N, number of collocation angles, number of terms in Grünwald series (18);
p, liquid pressure [kg/s^2 m];
p_v, vapour pressure [kg/s^2 m];
p_v^A, partial vapour pressure of more volatile component A [kg/s^2 m];
p_∞, liquid pressure far away from bubble [kg/s^2 m];
Pr, $= \nu/a$, Prandtl number;
q, heat flux [kg/s^3], number denoting order of fractional differentiation in equation (18);
q_M, heat flux at vapour–liquid interface in liquid microlayer [kg/s^3];
q_R, heat flux at vapour–liquid interface in bulk liquid [kg/s^3];
Q, total heat flow [kgm^2/s^3];
Q_c, total mass flow of more volatile component A [kg/s];
Q_M, total heat flow at vapour–liquid interface in liquid microlayer [kgm^2/s^3];
Q_R, total heat flow at vapour–liquid interface in bulk liquid [kgm^2/s^3];
r, radial coordinate [m];
r_m, minimum meniscus radius [m];
r_0, mean meniscus radius [m];
R, radial coordinate of vapour–liquid interface at bubble cap [m];

* Present address: Neratoom, P.O. Box 2244, 2509AE Den Haag, The Netherlands.

Ra, $= g\alpha\Delta T h^3/av$, Rayleigh number;
Ra_c, critical Rayleigh number;
R_c, bubble contact radius [m];
R_d, radius of dry area [m];
R_{eq}, $= (3V/4\pi)^{1/3}$, equivalent bubble radius [m];
Rs, $= g\beta\Delta C h^3/av$, "salinity" Rayleigh number;
t, time elapsed since start of bubble growth [s];
t_r, time at which bubble starts to cover solid wall at place r [s];
T, absolute temperature [K];
ΔT, temperature difference with respect to melting ice, increase in saturation temperature in binary mixture [K];
T_b, absolute bulk temperature [K];
T_v, vapour temperature in pure system [K];
T_v^*, parameter characterizing excess pressure in bubble [K];
T_M, temperature of vapour–liquid interface in liquid microlayer [K];
T_M^*, parameter in equation (34) [K];
T_R, temperature of vapour–liquid interface in bulk liquid [K];
T_R^*, parameter in equation (34) [K];
T_s, saturation temperature at pressure p_∞ [K];
T_w, temperature of superheated wall [K];
T_∞, temperature at edge of thermal boundary layer in bulk liquid [K];
$\bar{T}_\infty$, mean value of T_∞ [K];
$\mathbf{u}$, liquid velocity vector [m/s];
u_r, liquid velocity in radial direction [m/s];
u_0, liquid velocity in azimuthal direction [m/s];
V, bubble volume [m^3];
x, $= R_c - r$, radial coordinate along wall with origin at bubble contact radius [m];
X, mole fraction of more volatile component A in liquid B;
X_∞, mole fraction of more volatile component A at edge of diffusion boundary layer;
X_M, mole fraction of more volatile component A at vapour–liquid interface in liquid microlayer;
X_R, mole fraction of more volatile component A at vapour–liquid interface in bulk liquid;
Y, mole fraction of more volatile component A in vapour B;
z, $= r - R$, radial coordinate with origin at bubble cap, displacement of centre of spherical bubble due to buoyancy [m].

Greek symbols

α, volumetric thermal liquid expansion coefficient [1/K];
α_c, vapour–liquid–solid contact angle in triple interphase region;
β, volumetric salinity expansion coefficient [m^3/kg];
γ_M, correction factor for heat removal in liquid microlayer in binary mixture;
γ_R, correction factor for heat removal at bubble cap in binary mixture;
Γ, gamma function;
Γ_M, volumetric rate of vapour production at vapour–liquid interface in microlayer [m^3/s];
Γ_R, volumetric rate of vapour production at vapour–liquid interface in bulk liquid [m^3/s];
δ, thermal boundary-layer thickness around bubble cap [m];
η, liquid dynamic viscosity [kg/s m];
η_s, $= 2\eta/h(R_d)$, slip viscosity at vapour–liquid–solid interfacial line [kg/s m^2];
θ, azimuthal coordinate;
θ_0, $= T_w - T_s$, wall superheating [K];
$\Delta\theta_0$, $= T_b - T_s$, bulk superheating [K];
μ, $= \cos\theta$, azimuthal cosine;
ν, liquid kinematic viscosity [m^2/s];
ρ, liquid density [kg/m^3];
ρ_v, vapour density [kg/m^3];
ρ_{vm}, vapour density in gas–vapour mixture [kg/m^3];
ρ_{gm}, gas density in gas–vapour mixture [kg/m^3];
σ, surface tension coefficient [kg/s^2];
τ, $= aJa^2/C_0^2$, characteristic time for transitional growth [s];
ϕ, liquid velocity potential [m^2/s].

1. INTRODUCTION

BECAUSE of its importance for practical applications, heat transfer from a horizontal heated wall to a fluid has been investigated frequently. One of the most interesting features in this configuration is the occurrence of buoyancy effects in the fluid. Buoyancy forces arise as a result of variations of density in a fluid subject to gravity.

Well-known is the Bénard problem [1], where density differences are caused by variations in temperature, i.e. $\Delta\rho = -\rho\alpha\Delta T$. It has been shown by Rayleigh [2] that the so-called Rayleigh number $Ra = g\alpha\Delta T h^3/av$ plays a dominating part in the stability properties of the Bénard problem: when Ra is larger than a critical Rayleigh number Ra_c, the flow is unstable and heat transport by natural convection occurs.

A comparatively recent development in the field of natural convection has been the study of fluids in which there are gradients of two (or more) properties with different molecular diffusivities. This is the case in a binary mixture and the variation in density is given by $\Delta\rho = -\rho\alpha\Delta T + \rho\beta\Delta C$. The stability properties of this system have been treated by Baines and Gill [3]. Their results show that both the Rayleigh number Ra, a so-called "salinity" Rayleigh number $Rs = g\beta\Delta C h^3/av$, the ratio of diffusivities D/a and

the Prandtl number ν/a determine the stability properties. For $Pr = 10$, $D/a = 10^{-2}$ (i.e. salt in water), Baines and Gill [3] present a diagram showing the stability properties as a function of Ra and Rs. In Section 2.1. the above mentioned results will be used.

Another well-known buoyancy problem is nucleate boiling, where density differences are caused by liquid–vapour phase transitions, initiated in small cavities at the wall (so-called heterogeneous nucleation). In practical applications, boiling heat transfer is often more advantageous than heat transport by natural convection, since in the former case the periodic growth and departure of vapour bubbles causes forced liquid convection, which contributes substantially more to heat transport than natural convection.

Unfortunately there is an upper limit in the heat-transfer rate. At a sufficiently high driving temperature difference, the number of bubbles at the superheated wall becomes so large that these vapour bubbles coalesce and form a coherent vapour film, insulating the wall from the liquid. These dry areas result in hot spots and eventually in deposition of salt, which leads to damage of the wall. For that reason investigations with the purpose to increase the peak flux are of great practical importance. In this paper special attention is paid to bubble departure.

In spite of the many empirical or semi-empirical correlations available, nucleate boiling heat transfer is much less understood than natural convection. This is mainly due to the limited knowledge available about the nucleation processes in a heterogeneous medium [4]. In this paper the nucleation process will not be considered.

In a well-known paper by Fritz [5], bubble departure is considered as a buoyancy phenomenon and the departure radius is calculated by a balance of surface tension and buoyancy forces. However, since vapour bubbles are growing, surface tension forces play a negligible part in comparison to inertia forces. In order to determine the departure radius as a consequence of buoyancy induced liquid acceleration, knowledge of the bubble growth rate is of essential importance, as has been shown by Maron-Moalem *et al.* [6].

In order to determine bubble growth rates Bošnjacović [7] simplified the hydrodynamics of the problem by the assumption that the bubble has a spherical shape and that the temperature in the bubble equals the saturation temperature T_s. Only conductive heat transfer in the liquid to the bubble cap was considered, resulting in:

$$R(t) = \frac{2}{\pi^{1/2}} Ja(at)^{1/2}, \tag{1}$$

where the dimensionless Jakob number equals:

$$Ja = \frac{\rho c(T_\infty - T_s)}{\rho_v l}. \tag{2}$$

Both Birkhoff, Margulies and Horning [8] and Scriven [9] corrected Bošnjacović's result by accounting for radial convection. They found a $3^{1/2}$ higher value for $R(t)$.

In a survey, Van Stralen [10], however, stressed that under many conditions, e.g. water boiling at subatmospheric pressures and liquid metals, the assumption $T_v = T_s$ is not correct and liquid inertia has to be included. In this way, for times immediately after nucleation, the following growth rate is found:

$$R(t) = \left[\frac{2}{3}\frac{\rho_v l}{\rho T_s}(T_\infty - T_s)\right]^{1/2} \cdot t = C_0 t. \tag{3}$$

Zijl *et al.* [11] derived an expression for transitional growth, showing that for $t \ll \tau = aJa^2/C_0^2$ the bubble growth rate is given by (3) and for $t \gg \tau$, $R(t)$ is given by (1). From their theory it is also seen that the temperature of the vapour in the bubble decreases gradually from $T_v = T_\infty$ for $t \ll \tau$ to $T_v = T_s$ for $t \gg \tau$.

Also for binary systems with a more volatile component, expressions have been derived and it is shown that for $t \gg \tau$ the bubble growth rate is much smaller than in a pure liquid under the same conditions, the reason being that the bubble temperature approaches a value $T_v = T_s + \Delta T$. The practical consequences of this slowing down effect have been stressed by Van Stralen [12], indicating that a smaller growth rate results in a smaller departure radius and consequently in a higher peak flux in nucleate boiling.

In principle the theories mentioned before only apply for free bubbles in an initially uniformly superheated liquid. Cooper and Lloyd [13] extended the theory derived in [7–9] to bubble growth at a horizontal superheated wall. Although, qualitatively speaking, the results do not differ so very much compared to the theory of free bubbles, the physics of this problem is much more complicated, mainly because of the existence of a thin liquid layer, the so-called evaporating microlayer, between the wall and the bubble. Van Ouwerkerk [14] improved the model developed in [13] using a similarity solution. Van Stralen *et al.* [15] accounted for the fact that the initial temperature field is not uniformly superheated and that growth may be inertia-controlled ($t \ll \tau$).

Knowing the bubble growth rate, Maron-Moalem *et al.* [6] approximated the departure radius with the aid of the "Kelvin-momentum" equation for spherical free bubbles:

$$\frac{1}{2}\frac{\mathrm{d}}{\mathrm{d}t}\left(\rho\frac{4}{3}\pi R^3 \dot{z}\right) = g\rho\frac{4}{3}\pi R^3. \tag{4}$$

Their results agree with experimental values, obtained in nucleate boiling at a liquid–liquid interface.

After bubble departure, cold bulk-liquid, with a temperature approximately equal to the saturation temperature, flows to the superheated wall. This liquid is heated, first only by conduction and after some time, when the thermal penetration thickness

has grown so large that the Rayleigh number Ra (or Ra and Rs) exceeds the critical value, also by natural convection. This process has been described by Han and Griffith [16]. They presented an expression for the waiting time, i.e. the time interval between bubble departure and nucleation.

Combination of the theory for the bubble growth rate [7–9], the theory for the departure time [6] and the theory for the waiting time [16] results in an expression for the bubble departure radius as a function of pressure $R_{dep} \sim 1/p$, as has been shown by Maron-Moalem and Zijl [17]. It turns out that the bubble departure radius is independent of the dimensions of the cavity in the wall, where the bubble is nucleated, the dependence on surface tension turns out to be the same as predicted by Fritz [5]. In this way relatively simple algebraic expressions have been obtained to describe buoyancy effects in a fluid, heated from below, where phase transitions take place at the wall.

However, from a physical point of view the picture obtained in this way is not fully satisfactory since in all the theories described before, deviations from the spherical bubble shape have been neglected; i.e. the hydrodynamics of free spherical bubbles has been applied.

Deviations from the spherical bubble shape have been treated by Zijl [18] for gas bubbles and by Joosten *et al.* [19] for vapour bubbles. The latter authors neglected the existence of an evaporating microlayer and presented only a crude approximation of the heat-transfer process at the bubble cap.

In the present paper the hydrodynamics of the problem will be solved by the global orthogonal collocation method, as has been done in [18, 19]. The heat-transfer process, however, both in the evaporating microlayer and at the bubble cap, will be treated in much more detail. For that purpose use has been made of the fractional calculus.

Integrals of fractional order have been applied for the first time by Abel in 1823 for the tautochrone problem. In 1920 Heaviside used this concept in electromagnetic theory (see [20]). In the field of electrochemistry Oldham and Spanier [21] extended this theory and presented examples of how to solve complicated diffusion problems in a simple way. An example using their theory for growth, oscillations and implosion of a spherical free vapour bubble has been presented by Zijl *et al.* [11]. In this paper the formalism of fractional calculus will be used to derive equations which can easily be applied in standard routines for numerical integration of sets of ordinary differential equations. The numerical results presented here have been compared with experimental data obtained in pure water and water–butanone mixtures at subatmospheric pressures. The results are in quantitative agreement.

2. THE EVAPORATING LIQUID MICROLAYER

2.1. *Hydrodynamics of the liquid microlayer*

During the time that the bubble contact radius R_c is growing, a thin layer of liquid remains at the heated wall. This liquid layer is a consequence of the no-slip boundary condition at the wall for the hydrodynamic equations of continuity and conservation of momentum.

The actual thickness of formation at $r = R_c$, however, is determined by the boundary condition at the vapour–liquid interface, expressing that the liquid normal stress equals the surface tension, caused by curvature of the vapour–liquid interface.

This process of liquid microlayer formation has been discussed by Zijl [22, 23]. A modified equation of Landau and Levich [24] for the free coating problem has been proposed in order to calculate the thickness of formation h_0 and the radius of curvature r_0 in the meniscus region,† see Fig. 1. The result of Landau and Levich is:

$$h_0 = 1.333\left(\frac{\eta}{\sigma}\dot{R}_c\right)^{2/3} r_m. \tag{5}$$

The expression to determine r_m is given by:

$$\sigma \frac{\dfrac{d^2h}{dx^2}}{\left[1+\left(\dfrac{dh}{dx}\right)^2\right]^{2/3}} = \rho\left[-\ddot{R}_c x + 3\left(\frac{\dot{R}_c}{R_c}\right)^2 x^2\right], \tag{6}$$

where the term in the RHS of (6) (the pressure caused by system acceleration) replaces the term $\rho g x$ (the pressure caused by gravitational acceleration) in Landau and Levich's [24] result. Integration of equation (6) results in:

$$\frac{\dfrac{dh}{dx}}{\left[1+\left(\dfrac{dh}{dx}\right)^2\right]^{1/2}} = \frac{\rho}{2\sigma}\left|-\ddot{R}_c x^2 + 2\left(\frac{\dot{R}_c}{R_c}\right)^2 x^3\right| - 1. \tag{7}$$

The value of x where $dh/dx = 0$ is given by:

$$x = f(a,b,c) = \begin{cases} f_0(a,b,c) \text{ if } \dfrac{4b^3}{27a^2c} \leqslant 1 \\ f_\infty(a,b,c) \text{ if } \dfrac{4b^3}{27a^2c} \geqslant 1, \end{cases} \tag{8a}$$

where

$$f_0(a,b,c) = -\frac{b}{3a} + \left(\frac{c}{a}\right)^{1/3}\left[\frac{1}{2} - \frac{b^3}{27a^2c} + \left(\frac{1}{4} - \frac{b^3}{27a^2c}\right)^{1/2}\right]^{1/3} + \left(\frac{c}{a}\right)^{1/3}\left[\frac{1}{2} - \frac{b^3}{27a^2c} - \left(\frac{1}{4} - \frac{b^3}{27a^2c}\right)^{1/2}\right]^{1/3} \tag{8b}$$

†The analogy between the formation of a thin liquid layer beneath a growing bubble and at a moving plate has been suggested independently by Professor G. A. Sparenberg of the Groningen State University during a meeting of the Dutch subgroup "Two-phase flow".

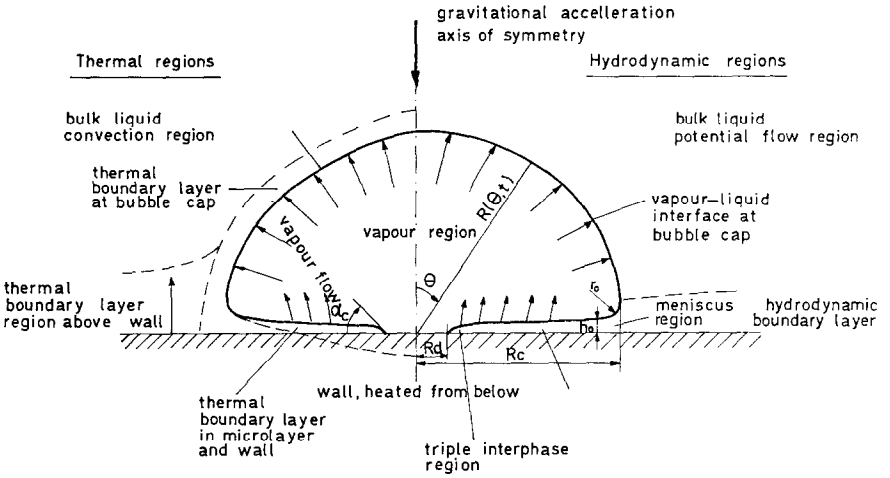

FIG. 1. Rotational symmetric vapour bubble growing at a superheated horizontal wall. On the left the thermal regions and on the right the hydrodynamic regions are indicated.

and

$$f_\infty(a,b,c) = -\frac{b}{3a} + \frac{b}{3a}\cos\left[\frac{1}{3}\arccos\left(1-\frac{27a^2c}{2b^3}\right)\right] + \frac{b(3)^{1/2}}{3a}\sin\left[\frac{1}{3}\arccos\left(1-\frac{27a^2c}{2b^3}\right)\right]. \quad (8c)$$

In these expressions $a = 2(\dot{R}_c/R_c)^2$, $b = -\ddot{R}_c$ and $c = 2\sigma/\rho$.

Substitution of (8a) into (6) results in the required expression for $r_m = 1/(\mathrm{d}^2h/\mathrm{d}x^2)_{\mathrm{d}h/\mathrm{d}x=0}$:

$$r_m = \frac{c}{f(3af+2b)}. \quad (9)$$

According to Groenveld [25] the mean radius of curvature r_0 is best approximated by $r_0 = 3r_m$.

In a binary mixture, the experimentally determined microlayer thickness turns out to be more than two times thicker than the value predicted by expression (5), see Section 5. This so-called "water paradox" has been explained quantitatively by Groenveld [25], who showed that surface tension gradients along the meniscus (see Section 3), enabling the interface to support tangential stresses, result in an increase of the value for h_0 by a factor of 2.753.

After formation of this layer at $r = R_c$ the thickness decreases for two reasons:

(i) Especially in the triple interphase region at $r = R_d$ the vapour–liquid interface is curved. The associated surface tension force sets the liquid into motion and drives the liquid out of the layer. This results in a decrease of thickness.

(ii) Since the temperature of the microlayer is, in general, higher than the temperature of the vapour, a heat flux flows from that layer to the vapour–liquid interface, causing vaporization of liquid. The vapour produced in this way is an important cause of bubble growth and is also a reason for the decrease in layer thickness.

Under the assumption that the Bond number $\rho g h^2/\sigma \ll 1$, the following equation, accounting for these two effects has been derived by Zijl [22, 23]:

$$\frac{\partial h}{\partial t} = \frac{2}{3}\frac{\sigma}{\eta}\frac{h^3}{r^2}\frac{\partial^2 h}{\partial r^2} - \frac{q}{\rho l}, \quad (10)$$

where the first term in the RHS accounts for the effects mentioned in (i) and the second term in the RHS for the effects in (ii). With the auxiliary conditions that at $r = R_d$, $h = 2\eta/\eta_s$ and $\partial h/\partial r = \tan\alpha_c$ and at $r = R_c$, $h = h_0$, an approximate solution is presented by Zijl [32] for the dry area radius $R_d(t)$ as a function of time. From this result it is observed that in water, boiling at subatmospheric pressures, the first term in the RHS of (10) may be neglected with respect to the second term in the RHS for not too low values of the "slip viscosity" η_s. Furthermore it is derived that $R_d \ll R_c$ during the time that R_c is growing.

In the deviations of (5,..., 10) steady Stokes flow and negligible gravity has been assumed. As has been pointed out in the introduction, gravity may result in a Bénard instability. However, in almost all cases the Rayleigh number is smaller than the critical Rayleigh number $Ra_c = 27\pi^4/4 \simeq 657$ for this case.

Since, as will be shown in Section 2.2., evaporation takes place at $r = R_c$ at a higher rate than at $r = R_d$, there is a vapour shear flow from R_c to R_d, setting the film into motion. In addition, in a binary system there is a concentration gradient at the vapour–liquid interface resulting in a gradient of surface-tension in the direction from R_c to R_d. Also this gradient sets the film into motion. Such a flowing film is unstable and may break up. This effect is damped by surface tension.

A third cause of instability has been reported by Mesler [26], who showed the existence of ebullition of small vapour bubbles in the microlayer.

In the following only stable microlayers will be considered.

2.2. *Heat transport in a stable liquid microlayer*

In this Section the formalism of fractional calculus will be used, see Oldham and Spanier [21].

Let us consider what happens at a prescribed plate r from the axis of symmetry of the bubble. At a certain time t_r after start of bubble growth, the bubble covers the place r and a microlayer is formed. This time is determined by the implicit relationship:

$$R_c(t_r) = r. \tag{11}$$

Since the temperature of the vapour at the interface $T_M(t)$ is in general lower than the temperature of the wall T_w and consequently also of the temperature of the liquid microlayer at the moment when it is formed, heat will start flowing from this layer to the vapour–liquid interface. According to Oldham and Spanier [21] the heat flux at the (plane) interface at place r equals:

$$q_M(t) = \begin{cases} 0 & t < t_r \\ -\rho c a^{1/2} \dfrac{\mathrm{d}^{1/2}}{\mathrm{d}(t-t_r)^{1/2}} [T_M(t) - T_w], & \\ & t > t_r. \end{cases} \tag{12}$$

In principle, equation (12) is only valid not too far from $r = R_c$, where the penetration thickness for heat diffusion is small compared to the microlayer thickness. In that region the highest instantaneous heat flux occurs, consequently this region contributes dominantly to the vapour production. For that reason it is approximated that equation (12) is valid over the whole surface from $r = 0$ to $r = R_c$. In this way also the existence of a small dry area is neglected.

From expression (12) the total heat flow to the vapour–liquid interface can be calculated by integration over the wetted surface:

$$Q_M(t) = -2\pi\rho c a^{1/2} \int_{r=0}^{R_c(t)} r \frac{\mathrm{d}^{1/2}}{\mathrm{d}[t - t_r(r)]^{1/2}} \times [T_M(t) - T_w]\,\mathrm{d}r. \tag{13}$$

Only when $\dot{R}_c > 0$, i.e. when the bubble covers new hot liquid in the microlayer, can equations (11) and (13) be combined, resulting in:

$$Q_M(t) = -2\pi\rho c a^{1/2} \int_{t_r=0}^{t} R_c(t_r)\dot{R}_c(t_r) \times \frac{\mathrm{d}^{1/2}}{\mathrm{d}(t-t_r)^{1/2}} [T_M(t) - T_w]\,\mathrm{d}t_r. \tag{14}$$

The heat flow Q_M causes evaporation of the liquid microlayer, consequently a flow of vapour mass Q_M/l "blows" into the bubble. Since the liquid is much denser than the vapour, the bubble volume increases much more (a factor ρ/ρ_v) than the volume of the microlayer decreases. When vapour production at the bubble cap is neglected it follows from (14) that the growth rate of the bubble volume is given by:

$$\dot{V}(t) = -\pi \frac{\rho c}{\rho_v l} a^{1/2} \int_{t_r=0}^{t} \mathrm{d}R_c^2(t_r)/\mathrm{d}t \times \frac{\mathrm{d}^{1/2}}{\mathrm{d}(t-t_r)^{1/2}} [T_M(t) - T_w]\,\mathrm{d}t_r. \tag{15}$$

When, from the hydrodynamics in the liquid, the coordinates of the vapour–liquid interface at the bubble cap are known as a function of time (see Section 5) $V(t)$ and $R_c(t)$ are known and equation (15) has to be used to determine the unknown vapour temperature at the interface $T_M(t)$. In order to do this, an approximation is introduced.*

It was argued before that the most important contribution to vapour production comes from times shortly after initial formation of the microlayer, i.e. for times $t \gtrsim t_r$. During this relatively short time interval, the vapour temperature does not change so very much and may be assumed to be constant. With the property $\mathrm{d}^{1/2}1/\mathrm{d}t^{1/2} = 1/(\pi t)^{1/2}$ and the Riemann–Liouville definition of fractional integrals [21], equation (15) is transformed to:

$$\dot{V}(t) = -\pi \frac{\rho c}{\rho_v l} a^{1/2} \frac{\mathrm{d}^{-1/2}}{\mathrm{d}t^{-1/2}} \times \{[T_M(t) - T_w]\,\mathrm{d}R_c^2(t)/\mathrm{d}t\},$$

or, as an approximation:

$$\dot{V}(t) = -\pi \frac{\rho c}{\rho_v l} a^{1/2} \frac{\mathrm{d}^{-1/2}}{\mathrm{d}t^{-1/2}} \frac{\mathrm{d}}{\mathrm{d}t} \{[T_M(t) - T_w] R_c^2\}.$$

This equation has to be transformed in such a way that it can easily be used in a standard routine for numerical integration of sets of ordinary differential equations. For that purpose, use will be made of the composition rule $\mathrm{d}^{1/2} f = \mathrm{d}^{-1/2}\mathrm{d}f + f(0)/(\pi t)^{1/2}$, where $f(0) = [T_M - T_w]R_c^2$ is assumed to be equal to zero. In this way one yields:

$$T_M(t) - T_w = -\frac{\rho_v l}{\rho c a^{1/2}} \frac{1}{\pi R_c^2} \frac{\mathrm{d}^{-1/2}}{\mathrm{d}t^{-1/2}} \dot{V}. \tag{16}$$

Taking the square of this expression and differentiation with respect to time results in:

$$\frac{\mathrm{d}}{\mathrm{d}t}(T_M - T_w)^2 = \left(\frac{\rho_v l}{\rho c}\right)^2 \frac{1}{2\pi^2 a} \frac{\mathrm{d}^{-1/2}\dot{V}}{\mathrm{d}t^{-1/2}} \frac{\mathrm{d}^{1/2}\dot{V}}{\mathrm{d}t^{-1/2}}, \tag{17}$$

where the composition rule $\mathrm{d}\mathrm{d}^{-1/2} f = \mathrm{d}^{1/2} f$ has been applied.

Now use will be made of the Grünwald definition of fractional derivatives and integrals [21]:

$$\frac{\mathrm{d}^q f}{\mathrm{d}t^q} = \lim_{N\to\infty} \left(\frac{t}{N}\right)^{-q} \frac{1}{\Gamma(-q)} \times \sum_{j=0}^{N-1} \frac{\Gamma(j-q)}{\Gamma(j+1)} f\left(t - j\frac{t}{N}\right). \tag{18}$$

* Equation (16) can be derived exactly from equation (15) by more complex analysis.

Substitution of equation (18) for $q = -\frac{1}{2}$ and $q = \frac{1}{2}$ in the RHS of (17) results in:

$$\frac{\mathrm{d}}{\mathrm{d}t}[R_c(T_M - T_w)]^2 = \frac{1}{\pi^2 a}\frac{\rho_v l}{\rho c}[\dot{V}(t)+E_p][\dot{V}(t)-E_m], \quad (19.1)$$

$$E_p = \frac{1}{\pi^{1/2}} \lim_{N\to\infty} \sum_{j=1}^{N-1} \frac{\Gamma(j+\frac{1}{2})}{\Gamma(j+1)} \dot{V}\left(t - j\frac{t}{N}\right), \quad (19.2)$$

$$E_m = \frac{1}{2\pi^{1/2}} \lim_{N\to\infty} \sum_{j=1}^{N-1} \frac{\Gamma(j-\frac{1}{2})}{\Gamma(j+1)} \dot{V}\left(t - j\frac{t}{N}\right). \quad (19.3)$$

As a numerical approximation, the number of $N-1$ memory points for $\dot{V}$ will be taken finite. For the computation of the memory series (19.2,3), the values of $\dot{V}$ have to be stored at equidistant time intervals. However, the integration of equation (19.1) may be performed with any subdivision of these intervals, required in the numerical integration procedure.

In the general case that vaporization also takes place at the bubble cap, the growth rate of the bubble volume $\dot{V}$ in equations (15)–(19) has to be replaced by the volumetric vapour flux Γ_M, denoting the volumetric rate of vapour production at the vapour–liquid interface in the evaporating microlayer.

3. COMBINED EFFECT OF VAPORIZATION AT MICROLAYER AND BUBBLE CAP

3.1. *The thermal boundary layer at the bubble cap*

The process of heat transfer to the bubble cap is much harder to describe than the heat transport process to the vapour–liquid interface in the evaporating liquid microlayer. This is due to the following:

(i) The bubble cap is not flat, but curved.

(ii) Since the bubble cap is moving, heat transport does not only take place by conduction, but also by convection.

(iii) The bubble is surrounded by a non-uniformly superheated liquid.

Because of these reasons the solution around the bubble cap will have a more approximate character than in the case of the evaporating microlayer.

The heat transport equation in rotationally symmetric spherical coordinates equals:

$$\left(\frac{\partial}{\partial t} + u_r\frac{\partial}{\partial r} + \frac{u_\theta}{r}\frac{\partial}{\partial \theta}\right)T = a\left(\frac{\partial^2}{\partial r^2} + \frac{2}{r}\frac{\partial}{\partial r} + \frac{1}{r^2}\frac{\partial^2}{\partial \theta^2} + \frac{1}{r^2}\cot\theta\frac{\partial}{\partial\theta}\right)T. \quad (20)$$

When there was no buoyancy force, the bubble would never depart from the wall and always kept its initial hemispherical shape. As an approximation this situation will be used for the solution of equation (20). In that case the terms with $\partial/\partial\theta$ cancel.

It is convenient to transform to a new coordinate $z = r - R(t)$ moving with the velocity of the hemispherical bubble cap. In this coordinate system the spherical symmetric equation (20) becomes:

$$\frac{\partial T}{\partial t} - \frac{z(z+2R)}{(z+R)^2}\dot{R}\frac{\partial T}{\partial z} = a\left(\frac{\partial^2 T}{\partial z^2} + \frac{2}{z+R}\frac{\partial T}{\partial z}\right). \quad (21)$$

In a very thin boundary layer $z/R \to 0$ and equation (21) reduces to the heat-diffusion equation:

$$\frac{\partial T}{\partial t} = a\left(\frac{\partial^2 T}{\partial z^2} + \frac{2}{z+R}\frac{\partial T}{\partial r}\right). \quad (22)$$

According to Oldham [27], the solution of (22) for the heat flux at the hemispherical bubble cap in the direction to the vapour–liquid interface equals:

$$q_R(t) = -\rho c a^{1/2}\frac{\mathrm{d}^{1/2}}{\mathrm{d}t^{1/2}}[T_R(t) - T_\infty] - \rho c a\frac{T_R(t)-T_\infty}{R(t)}. \quad (23)$$

Strictly speaking, expression (23) is only valid for time independent radius R and temperature $T_\infty(\theta)$ at the edge of the thermal boundary layer. However, since $T_\infty(t)$ changes slowly with respect to $T_R(t)$, the range of validity for (23) is assumed to be approximately valid for varying T_∞.

In a paper by Maron-Moalem and Zijl [17], it is proved that for large bubbles, occurring in water boiling at subatmospheric pressures, the second term in the RHS of equation (23), i.e. the curvature term, may be neglected. However, it is also proved there that the second term in the LHS of equation (21), i.e. the radial convection term, has the same order of magnitude as the first term in the RHS of (21).

In order to account for this, equation (23) (with negligible curvature term) is "corrected" by adding a factor $3^{1/2}$, see Introduction.

$$q_R(t) = -3^{1/2}\rho c a^{1/2}\frac{\mathrm{d}^{1/2}}{\mathrm{d}t^{1/2}}[T_R(t) - T_\infty]. \quad (24)$$

In case of a free vapour bubble under zero gravity conditions, in the mode of asymptotic diffusion controlled growth, where $T_R(t) = T_s$, equation (24) just reduces to equation (1), corrected with the factor $3^{1/2}$ obtained by Birkhoff *et al.* [8]. This result is obtained applying the heat flux requirement $q_R = \rho_v l\dot{R}$ and the semi-derivative of 1, $\mathrm{d}^{1/2}1/\mathrm{d}t^{1/2} = 1/(\pi t)^{1/2}$.

From expression (24) the total heat flow to the vapour–liquid interface can be calculated by integration over the surface of the bubble cap:

$$Q_R(t) = -2\pi 3^{1/2}\rho c a^{1/2}\int_{\theta=0}^{\pi/2} R^2(\theta,t) \times \sin\theta\frac{\mathrm{d}^{1/2}}{\mathrm{d}t^{1/2}}[T_R(t) - T_\infty(\theta,t)]\,\mathrm{d}\theta.$$

When vapour production at the evaporating microlayer is neglected, the amount of vapour, caused by vaporization of liquid at the bubble cap, blows up

the bubble. The volumetric growth rate $\dot{V} = Q_R/\rho_v l$ equals:

$$\dot{V}(t) = -2\pi 3^{1/2}\frac{\rho c}{\rho_v l}a^{1/2}\int_{\theta=0}^{\pi/2} R^2(\theta,t) \times \sin\theta \frac{\mathrm{d}^{1/2}}{\mathrm{d}t^{1/2}}[T_R(t)-T_\infty(\theta,t)]\,\mathrm{d}\theta. \quad (25)$$

When $T_\infty(\theta,t)$ is also a slowly varying function of θ, or when the bubble shape is almost spherical, the following relationship holds approximately:

$$\frac{\int_0^{1/2\pi} R^2(\theta,t)\sin\theta T_\infty(\theta,t)\,\mathrm{d}\theta}{\int_0^{1/2\pi} R^2(\theta,t)\sin\theta\,\mathrm{d}\theta} = \frac{\mathrm{d}^{-1/2}}{\mathrm{d}t^{-1/2}}\frac{\int_0^{1/2\pi} R^2(\theta,t)\sin\theta\frac{\mathrm{d}^{1/2}}{\mathrm{d}t^{1/2}}T_\infty(\theta,t)\,\mathrm{d}\theta}{\int_0^{1/2\pi} R^2(\theta,t)\sin\theta\,\mathrm{d}\theta}.$$

With the composition rule for $f(0) = 0$, $\mathrm{d}^{-1/2}\mathrm{d}^{1/2}f = f$ it is observed that this is exact for T_∞ independent of θ.

Substitution of this approximation into expression (25) results in:

$$\dot{V}(t) = -3^{1/2}\frac{\rho c}{\rho_v l}a^{1/2}A(t)\frac{\mathrm{d}^{1/2}}{\mathrm{d}t^{1/2}} \times [T_R(t)-\bar{T}_\infty(t)], \quad (26)$$

where the surface of the bubble cap is given by:

$$A(t) = 2\pi\int_{\theta=0}^{\pi/2} R^2(\theta,t)\sin\theta\,\mathrm{d}\theta, \quad (27)$$

and the mean temperature at the edge of the thermal boundary layer is given by:

$$\bar{T}_\infty(t) = \frac{2\pi}{A(t)}\int_{\theta=0}^{\pi/2} R^2(\theta,t)\sin\theta T_\infty(\theta,t)\,\mathrm{d}\theta. \quad (28)$$

Expression (26) can be rewritten as:

$$T_R(t)-\bar{T}_\infty(t) = -\frac{\rho_v l}{3^{1/2}\rho c a^{1/2}}\frac{\mathrm{d}^{-1/2}}{\mathrm{d}t^{-1/2}}\frac{\dot{V}(t)}{A(t)}. \quad (29)$$

In the same way as in Section 3.2., the Grünwald definition of fractional derivatives and integrals (18) can be used to transform (29) into expressions suitable for numerical integration. The result is:

$$\frac{\mathrm{d}}{\mathrm{d}t}(T_R-\bar{T}_\infty)^2 = \frac{1}{6\pi^2 a}\left(\frac{\rho_v l}{\rho c}\right)^2 \times \left[\frac{\dot{V}(t)}{A(t)}+G_p\right]\left[\frac{\dot{V}(t)}{A(t)}-G_m\right], \quad (30.1)$$

$$G_p = \frac{1}{\pi^{1/2}}\lim_{N\to\infty}\sum_{j=1}^{N-1}\frac{\Gamma(j+\frac{1}{2})}{\Gamma(j+1)}\left(\frac{\dot{V}}{A}\right)_{[t-j(t/N)]}, \quad (30.2)$$

$$G_m = \frac{1}{2\pi^{1/2}}\lim_{N\to\infty}\sum_{j=1}^{N-1}\frac{\Gamma(j-\frac{1}{2})}{(j+1)}\left(\frac{\dot{V}}{A}\right)_{[t-j(t/N)]}. \quad (30.3)$$

In the general case that vaporization also takes place at the vapour–liquid interface in the evaporating microlayer, the growth rate of the bubble volume $\dot{V}$ has to be replaced by the volumetric vapour flux Γ_R, denoting the volumetric rate of vapour production at the vapour–liquid interface of the bubble cap.

3.2. *The vapour temperature*

It is now assumed that the pressure in the vapour is homogeneous in space and only a function of time. When it is furthermore assumed that the vapour is in thermodynamic equilibrium with the adjacent liquid it follows from Clapeyron's law that (in a pure system) also the temperature of the vapour T_v is homogeneous in space, i.e. $T_M = T_R = T_v$. The assumption of homogeneous vapour temperature has been discussed by Kenning and Toral [28], who considered deviations from homogeneity in order to explain the occurrence of surface tension gradients along the vapour–liquid interface in a pure system.

Since $\dot{V} = \Gamma_M + \Gamma_R$, where $\dot{V}$ is known from the hydrodynamics of the problem, see Section 5, this set can in principle be solved for the two unknowns T_v and Γ_M (or Γ_R).

In a similar way as described in subsections 2.2. and 3.1. equation (16) can be transformed to an equation suitable for the numerical calculation of $\Gamma_M(t)$. Equation (30) is used for the determination of $T_v(t)$. However, it turned out that for numerical integration many timesteps were required, resulting in an intolerably high computation time. Also when equation (19) is used for determination of $T_v(t)$ and equation (29) for the determination of $\Gamma_M(t)$, the same difficulties can be expected. For that reason another reasonable approximation will be introduced.

The temperature calculated with expressions (19), where V is the real bubble volume, is defined as T_M^*. In the same way, the temperature defined by equations (30) is called T_R^*. In general T_M^* and T_R^* are only parameters which do not represent a physical temperature. Only in the limiting cases where the bubble cap or the microlayer do not play a part $T_M^* = T_v$, respectively $T_R^* = T_v$. Now an expression for T_v, continuously connecting both limiting cases, will be derived.

In subsection 3.1. it is derived that:

$$T_R^* = \bar{T}_\infty - \frac{1}{3^{1/2}\rho c a^{1/2}}\frac{\mathrm{d}^{-1/2}}{\mathrm{d}t^{-1/2}}\frac{Q}{A}. \quad (31)$$

If the heat flux q_M in the evaporating microlayer were homogeneous the following expression would be obtained instead of (16):*

$$T_M^* = T_w - \frac{1}{\rho c a^{1/2}}\frac{\mathrm{d}^{-1/2}}{\mathrm{d}t^{-1/2}}\frac{Q}{\pi R_c^2}. \quad (32)$$

It follows from (31) and (32) that the mean heat flux equals $Q/(3^{1/2}A+\pi R_c^2)$, and consequently the following

*In [23] it is shown that replacement of πR_c^2 by $2\pi R_c^2$ in equation (32) results in a better approximation.

expression is approximately true:

$$T_v = \frac{3^{1/2}A\bar{T}_\infty + \pi R_c^2 T_w}{3^{1/2}A + \pi R_c^2} = \frac{1}{\rho c a^{1/2}} \frac{d^{-1/2}}{dt^{-1/2}} \frac{Q}{3^{1/2}A + \pi R_c^2}. \quad (33)$$

Initially after start of bubble growth contraction of the bubble foot does hardly take place, i.e. the bubble keeps its hemispherical shape and the ratio $A/\pi R_c^2$ is constant. In that case it follows from (31–33) that:

$$T_v = \frac{1}{2} \frac{3^{1/2}A(T_R^* + \bar{T}_\infty) + \pi R_c^2 (T_M^* + T_w)}{3^{1/2}A + \pi R_c^2}. \quad (34)$$

As an approximation, expression (34) is used to calculate T_v from the values of T_M^* and T_R^*, obtained by the numerical integration of (19) respectively (30). In this way a very efficient numerical algorithm has been obtained.

4. EXTENSION TO BINARY MIXTURES

In view of practical applications (heat exchangers, nuclear reactors), great efforts have been made to increase the maximum nucleate boiling heat flux, e.g. by an elevation of pressure and by the introduction of forced convection, both in combination with a subcooling of the bulk liquid. Maron-Moalem *et al.* [6] proposed the idea of nucleate boiling at a liquid–liquid interface of two immiscible liquids. Bubble generation occurs then in close proximity of the heated solid wall and the onset of film boiling at the wall is prevented.

Another idea is to use a miscible binary mixture. At low concentrations of the more volatile component, the bubble frequency has been increased in combination with a diminishing tendency for bubble coalescence. The aspect of higher bubble frequency will be discussed in this subsection.

When a more volatile component A is added to the liquid B, both in the liquid microlayer and at the bubble cap, diffusion of this component to the vapour–gas phase takes place. Diffusion at the bubble cap has been treated by Zijl *et al.* [11], consequently only diffusion in the evaporating microlayer will be treated here in more detail.

According to the theory described in Section 2.2., the total heat flow Q to the vapour–liquid interface satisfies the following expression, see equation (16):

$$\pi R_c^2 (T_M - T_w) = -\frac{1}{\rho c a^{1/2}} \frac{d^{-1/2}Q}{dt^{-1/2}}. \quad (35)$$

In a similar way the following expression for the total flow Q_c of the more volatile component can be derived:

$$\pi R_c^2 (C_M - C_\infty) = -\frac{1}{D^{1/2}} \frac{d^{-1/2}Q_c}{dt^{-1/2}}. \quad (36)$$

Both by vaporization and by diffusion of the more volatile component into the bubble, the volumetric flux Γ_M of vapour–gas mixture into the bubble equals:

$$\Gamma_M = \frac{Q}{\rho_{vm} l_m} \quad \text{and} \quad \Gamma_M = \frac{Q_c}{\rho_{gm}},$$

where ρ_{vm} is the density of the vapour in the vapour–gas mixture and ρ_{gm} is the gas-phase density of the more volatile component in the mixture. It has been proved by van Stralen *et al.* [29] that $\rho_{vm} l_m = \rho_v l$, where ρ_v and l are the vapour density, respectively latent enthalpy of vaporization in a pure system under the same conditions. It has been proved by Maron-Moalem and Zijl [17] that $C = \rho(M_A/M_B)X$ and $\rho_{gm} = \rho_v(M_A/M_B)Y$, where X and Y are mole fractions of the more volatile component in the liquid and the vapour–gas mixture respectively.

Consequently, expressions (35, 36) result in the following equations:

$$\pi R_c^2 (T_M - T_w) = -\frac{\rho_v l}{\rho c a^{1/2}} \frac{d^{-1/2}\Gamma_M}{dt^{-1/2}}, \quad (37)$$

$$\pi R_c^2 (X_M - X_\infty) = -\frac{p_v^A \rho_v}{D^{1/2} p_\infty \rho} \frac{d^{-1/2}(X_R \Gamma_M)}{dt^{-1/2}}. \quad (38)$$

In the derivation of (38) use has been made of Dalton's law:

$$Y = \frac{p_v^A(T_R)}{p_v(T_R)} X_M \simeq \frac{p_v^A(T_s)}{p_\infty} X_M.$$

After linearization of (38) by putting

$$d^{-1/2}(X_M \Gamma_M)/dt^{-1/2} = X_M \, d^{-1/2}\Gamma_M/dt^{-1/2}$$

(see [11] for the validity of this linearization), the following expression is found after elimination of Γ_M from (37, 38).

$$X_M - X_\infty = \frac{\left(\frac{a}{D}\right)^{1/2} \frac{p_v^A}{p_\infty} \frac{c}{l} (T_M - T_w)}{1 - \left(\frac{a}{D}\right)^{1/2} \frac{p_v^A}{p_\infty} \frac{c}{l} (T_M - T_w)} X_\infty. \quad (39)$$

It has been derived in [11] by use of Clapeyron's and Raoult's laws in linearized form, that for the vapour–gas pressure p_v, which is again assumed to be homogeneous in the whole bubble, the following expression holds:

$$p_v - p_\infty = \frac{\rho_v l}{T_s} (T_M - T_s) + p_v^A(T_s)(X_M - X_\infty). \quad (40)$$

Substitution of (39) into (40) results in:

$$p_v - p_\infty = \frac{\rho_v l}{T_s} (T_v^* - T_s), \quad (41)$$

where T_v^* is defined as:

$$T_v^* - T_s = (1 + \gamma_M)(T_M - T_s) - \gamma_M (T_w - T_s) \quad (42)$$

and γ_M is defined as:

$$\gamma_M(T_M) = \frac{\left(\frac{a}{D}\right)^{1/2} \left(\frac{p_v^A}{p_\infty}\right)^2 \frac{c}{l} \frac{T_s}{\rho_v l} p_\infty X_\infty}{1 + \left(\frac{a}{D}\right)^{1/2} \frac{p_v^A}{p_\infty} \frac{c}{l} (T_w - T_M)}. \quad (43)$$

Combination of (37) and (42) results in:

$$\pi R_c^2(T_v^* - T_w) = -\frac{[1+\gamma_M(T_v^*)]\rho_v l}{\rho c a^{1/2}} \frac{\mathrm{d}^{-1/2}\Gamma_M}{\mathrm{d}t^{-1/2}}, \quad (44)$$

where $\gamma_M(T_v^*)$ can be determined algebraically by expressions (42, 43).

In the same way it can be proved that in a binary system equation (29) has to be replaced by [11]:

$$T_R - \bar{T}_\infty = -\frac{[+\gamma_R(T_v^*)]\rho_v l}{3^{1/2}\rho c a^{1/2}} \frac{\mathrm{d}^{-1/2}}{\mathrm{d}t^{-1/2}}\left(\frac{\Gamma_R}{A}\right), \quad (45)$$

where equation (41) is the same and in equations (42, 43) $\gamma_M \to \gamma_R$, $T_M \to T_R$ and $T_w \to \bar{T}_\infty$ ($\to$ means: has to be replaced by).

Since in a pure system expression (41) remains unchanged, with $T_v^* = T_v$, the description of the binary system has been reduced to the description of a pure system by replacing c in expressions (19), (30) by $c/(1+\gamma_M)$ and $c/(1+\gamma_R)$ respectively.

It is noteworthy to mention here that since in general $T_w \neq \bar{T}_\infty$, the temperatures and concentrations at the vapour–liquid interface in the microlayer and at the bubble cap are not equal, i.e. $T_M \neq T_R$, $X_M \neq X_R$, see equation (42). This fact will result in gradients in surface tension over the vapour–liquid interface in the meniscus region, leading to additional flow around the bubble, see Kenning and Toral [27]. In Section 2 this effect has been accounted for by Groenveld's correction in expression (5) [25].

5. CONVECTION AND HYDRODYNAMICS OF THE BULK LIQUID

If it is assumed that the vapour, produced at the vapour–liquid interface in the evaporating microlayer, arrives homogeneously at the bubble cap $R(\theta, t)$, the vapour velocity at $r = R(\theta, t)$ equals Γ_M/A. The normal displacement of the bubble cap per unit of time equals the normal velocity of the liquid at the bubble cap $(\mathbf{u}\cdot\mathbf{n})_{r=R}$. In this way the local heat requirement at $r = R(\theta, t)$ equals $q_R = \rho_v l[(\mathbf{u}\cdot\mathbf{n})_{r=R} - \Gamma_M/A]$ and the heat flux for $r > R$ (i.e. for $z > 0$) is given by, see Carslaw and Jaeger [29]:

$$q(z) = \frac{3^{1/2}\rho_v l}{\rho c a^{1/2}\pi^{1/2}} \int_{t'=0}^{t} \frac{\exp\left[-\dfrac{z^2}{4a(t'-t)}\right]}{(t'-t)^{1/2}} \times [(\mathbf{u}\cdot\mathbf{n})_{r=R} - \Gamma_M/A]_{t=t'}\,\mathrm{d}t'. \quad (46)$$

Γ_M/A can be determined by expression (24) and $(\mathbf{u}\cdot\mathbf{n})_{r=R}$ follows from the hydrodynamic equations. The thickness $z = \delta(\theta, t)$ where $q(z)/q_R = 5\%$, can be determined numerically and the bulk temperature at that place from the bubble cap is considered to be equal to $T_\infty(\theta, t)$, needed for the solution of expression (30) with the aid of (28).

In the bulk liquid, that is the liquid at the edge and outside the thermal boundary layer, temperature gradients are not so large and heat transport is considered to take place only by convection. In this way equation (20) reduces to:

$$\left(\frac{\partial}{\partial t} + u_r\frac{\partial}{\partial r} + \frac{u_\theta}{r}\frac{\partial}{\partial \theta}\right)T = \frac{DT}{Dt} = 0. \quad (47)$$

Equation (47) expresses that the temperature does not change along a streamline. Consequently, when the initial temperature distribution is prescribed, the temperature field for $t > 0$ can easily be determined when the flow field in the liquid around the bubble is known.

The determination of this flow field and consequently the coordinates of the bubble boundary have been described in detail by Zijl [18, 22] and Joosten *et al.* [19]. Consequently only a short summary will be presented here:

From a hydrodynamic point of view the heating surface is considered as a plane of symmetry between the bubble and its surrounding flow field and a "mirror" bubble and "mirror" flow field. In this way the normal velocity condition at the wall $(\mathbf{u}\cdot\mathbf{n})_w = \mathbf{0}$ is satisfied automatically. The no-slip condition at the wall does not play a part since for the large vapour bubbles under consideration, the liquid moves smoothly over a very thin viscous boundary layer, which does not affect the bulk flow and the bubble shape. The contact angle only plays a part in the evaporating microlayer, see Fig. 1.

In addition it is assumed that the influence of the tangential stress condition at the bubble boundary is only limited to a thin hydrodynamic boundary layer around the bubble. For a pure system this is a reasonable assumption, based on the absence of a wake region behind a non-translating bubble. For a binary system, however, the validity of this assumption is questionable since large gradients in tangential stress, introduced by gradients in surface tension, may cause additional flow phenomena.

Under the above mentioned restrictions, potential flow theory may be applied in the bulk liquid. Combination of the Bernouilli equation for the liquid pressure, the Laplace equation for the surface tension and expression (41) results in the following boundary condition for the potential equation for the velocity potential $\nabla^2\phi = 0$ [18, 19, 22]:

$$\frac{\partial\phi}{\partial t} = -\frac{1}{2}\left[\left(\frac{\partial\phi}{\partial r}\right)^2 + \left(\frac{1}{R}\frac{\partial\phi}{\partial\theta}\right)^2\right] - \frac{\rho_v l}{\rho T_s}(T_R^* - T_s) - g\frac{\rho-\rho_v}{\rho}R\cos\theta + \frac{\sigma}{\rho}\frac{1}{R}\left[\frac{1+2\left(\frac{1}{R}\frac{\partial R}{\partial\theta}\right)^2 - \frac{1}{R}\frac{\partial^2 R}{\partial\theta^2}}{1+\left(\frac{1}{R}\frac{\partial R}{\partial\theta}\right)^2} + 1 - \frac{1}{R}\frac{\partial R}{\partial\theta}\frac{\cos\theta}{\sin\theta}\frac{1}{\left[1+\left(\frac{1}{R}\frac{\partial R}{\partial\theta}\right)^2\right]^{1/2}}\right]. \quad (48)$$

The term $g(\rho-\rho_v)R\cos\theta$ represents the buoyancy term. This is the only place where this term occurs and deviations from the spherical bubble shape, i.e. contraction of the bubble foot and ultimately departure, are only due to this term.

The solution of potential equation $\nabla^2\phi = 0$, satisfying $(\mathbf{u}\cdot\mathbf{n})_w = 0$ equals

$$\phi(r,\theta,t) = \sum_{k=0}^{\infty} a_k(t)\frac{1}{r^{2k+1}}P_{2k}(\cos\theta).$$

As a numerical approximation, this series is cut after N terms. Instead of the N unknown expansion coefficients $[a_k(t)]_{k=0}^{N-1}$, N values of ϕ, $[\phi_i(t)]_{i=0}^{N-1}$ at N discrete angles θ_i (the so-called collocation angles) can be used. $\phi_i(t) = \phi[R(\theta_i,t),\theta_i,t]$

$$= \sum_{k=0}^{N-1}\left\{\frac{P_{2k}(\cos\theta_i)}{[R(\theta_i,t)]^{2k+1}}\right\}_{ik} a_k(t), \qquad i = O(1)N-1. \tag{49}$$

If boundary condition (48) is only used at these prescribed collocation points, a set of N ordinary differential equations is found for $\phi_i(t)$.

The condition that the flow velocity equals the displacement rate of the bubble boundary is expressed by:

$$\frac{\partial R}{\partial t} = \frac{\partial\phi}{\partial r} - \frac{1}{R^2}\frac{\partial R}{\partial\theta}\frac{\partial\phi}{\partial\theta} \quad \text{at } r = R(\theta,t). \tag{50}$$

If for every value of θ there is only one value for $R(\theta,t)$, also $R(\theta,t)$ may be expanded in even Legendre polynomials:

$$R(\theta,t) = \sum_{k=0}^{\infty} b_k(t)P_{2k}(\cos\theta).$$

In the same way, this series will be cut after N terms and instead of $[b_k(t)]_{k=0}^{N-1}$ the set $[R_i(t)]_{i=0}^{N-1}$ will be used, where b_k and R_i are related by the linear relationship:

$$R_i(t) = R(\theta_i,t) = \sum_{k=0}^{N-1}[P_{2k}(\cos\theta_i)]_{ik}b_k(t). \tag{51}$$

when boundary conditions (50) is only satisfied at the collocation angles θ_i, a set of ordinary differential equations is found for $R_i(t)$

It is noted that the $\mu_i = \cos\theta_i$ are chosen as the zeros of a Legendre polynomial. Only then convergence for $N\to\infty$ can be guaranteed [22]. The $2N$ ordinary differential equations, obtained in the way described above, combined with the two thermal ordinary differential equations (19, 30), result in a set of $2N+2$ coupled first order ordinary differential equations. This set can easily be solved by numerical standard routine. In the examples presented here an Euler method (without corrector) has been used. For every timestep the algebraic linear sets (49, 51) are solved by a Crout routine. In the examples presented in Section 6, the computation time at the Burroughs B7700 of the Eindhoven Technical University never exceeded 10 min.

6. THEORETICAL PREDICTIONS AND COMPARISONS TO EXPERIMENTAL RESULTS

6.1. *The numerical method*

The efficiency of numerical solution by the sets of equations (19), (30) will be first discussed for the simple case of a spherically symmetric vapour bubble in an initially uniformly superheated infinitely extended liquid in the absence of gravity. In that case only one term in the series (49), (51) is needed and the set (48), (50) reduces to the well-known second order Rayleigh equation [11], presented here as a set of two first order ordinary differential equations:

$$\frac{dR(t)}{dt} = \dot R(t), \tag{52.1}$$

$$\frac{d\dot R(t)}{dt} = \frac{-\frac{3}{2}\dot R(t)^2 + \frac{\rho_v l}{\rho T_s}[T_R(t)-T_s] - \frac{2\sigma}{\rho R(t)}}{R(t)}. \tag{52.2}$$

Since no evaporating microlayer is present, only equations (30) for $T_R(t)$ have to be solved simultaneously with expressions (52) for $R(t)$ and $\dot R(t)$. In this case $\dot V/A = \dot R$ and $\bar T_\infty = T_\infty$. $S(t)$ is defined as $S(t) = [T_R(t)-T_\infty]^2$, so that $T_R(t)-T_s$ in (52.2) equals $T_\infty - T_s - S(t)^{1/2}$.

The following set of equations is obtained in this way:

$$\frac{d\mathbf{Y}(t)}{dt} = \mathbf{F}(\mathbf{Y}),$$

where in this simple example $\mathbf{Y} = (R, \dot R, S)$.

In order to obtain a numerical solution, equidistant discrete timesteps Δt_2 are chosen and the time t equals $N\Delta t_2$, $N = 1,2,3,\ldots,\infty$. At these timepoints the values $\dot R[(N-j)\Delta t_2]$, $j = 1,2,\ldots,N-1$, needed in memory series (30.2,3), are stored. For the integration from $(N-1)\Delta t_2$ to $N\Delta t_2$, the interval Δt_2 may be subdivided into convenient timesteps $t_1 \leqslant t_2$; this is particularly useful in procedures with a self-finding timestep.

In this and further examples presented in this paper, a simple Euler method has been used:

$$\mathbf{Y}_N = \mathbf{Y}_{N-1} + \Delta t_1 \mathbf{F}(\mathbf{Y}_N).$$

In this way the set (52), (30) has been solved for a free vapour bubble, in water boiling at a pressure p_∞ of 20.28 kPa, see Fig. 2. R_1 has been calculated with $\Delta t_1 = \Delta t_2 = 40\,\mu s$.

R_2 has been calculated, initially, with half these timesteps, but after $N = 50$, 100, 150, etc. the steps are doubled and the values of $\dot R$ at memory places no longer needed have been skipped. In this way the computation time has been decreased more than ten times. When the memory series are omitted completely, the approximation introduced in [18, 19] is found.

6.2. *Dependence on initial values*

Van Stralen *et al.* [31] present experimentally determined bubble shapes and values of $R_{eq}(t)$ and $R_c(t)$ for pure water, boiling at 7.88 kPa (Fig. 6 in [31]). Corrected for the hydrostatic pressure of the

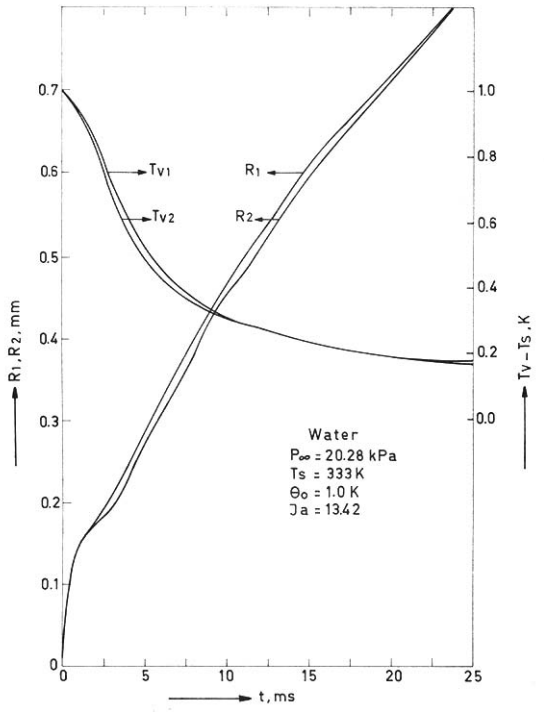

FIG. 2. Water boiling at 20.28 kPa. Comparison between the results of two procedures for the numerical calculation of the radius of a spherical bubble and the vapour superheating. The second, more economical, procedure (subscript: 2) gives only slightly different results, *cf.* text.

column of liquid above the superheated wall the pressure equals 10.38 kPa.

For this bubble, photographs, taken from a high speed motion picture are presented in Fig. 3. The numerically determined bubble shapes, where 3 collocation points have been used, are shown in Fig. 4.

Figure 5 shows $R_{eq}(t)$, $R_c(t)$ and $T_v(t)$ for $N = 3$ collocation points. Also, in case that $\dot{R}_c > 0$, the meniscus radius $r_0(t)$, calculated with expression (9) is presented.

Initially the liquid is motionless, i.e. $\phi(r,\theta,0) = 0$ and the initial bubble radius has been chosen equal to $R_i = 4\sigma T_s/\rho_v l(T_w - T_s)$. In this way the bubble starts growing, see equations (52). The initial temperature field has been chosen equal to:

$$T_\infty(z,0) = \begin{cases} T_w + (z/H)(T_s - T_w), & z \leqslant H \\ T_b & z \geqslant H, \end{cases} \tag{53}$$

where $T_b = T_s + \Delta\theta_0$ and $T_w = T_s + \theta_0$.

Such a linear temperature field is justified by experiments, see Section 6.3. The initial thickness H of the thermal boundary layer above the superheated wall has been chosen equal to 430 μm in order to fit the computed data to the experimental values.

Also experimental data for a water–2-Butanone mixture have been presented by van Stralen *et al.*, Figs. 8 and 9 [29]. The computed data are shown in Figs. 6 and 7.

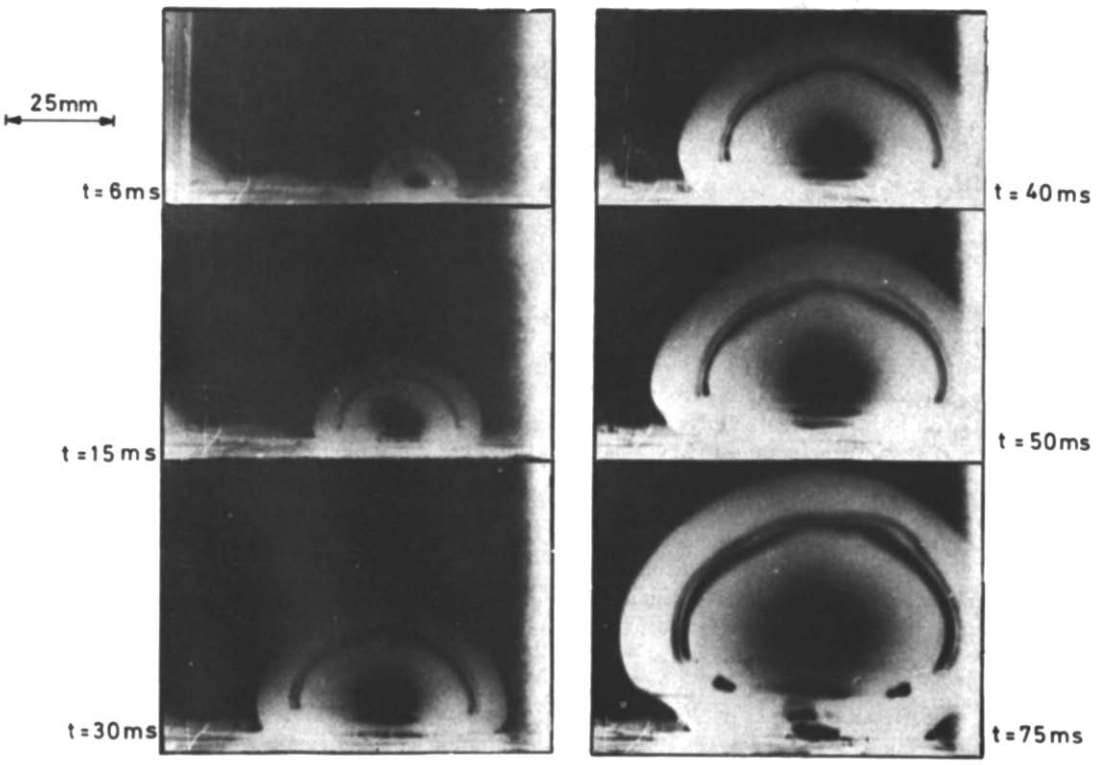

FIG. 3. Water boiling at 10.38 kPa. Photographs taken from a high speed motion picture, *cf.* Fig. 5.

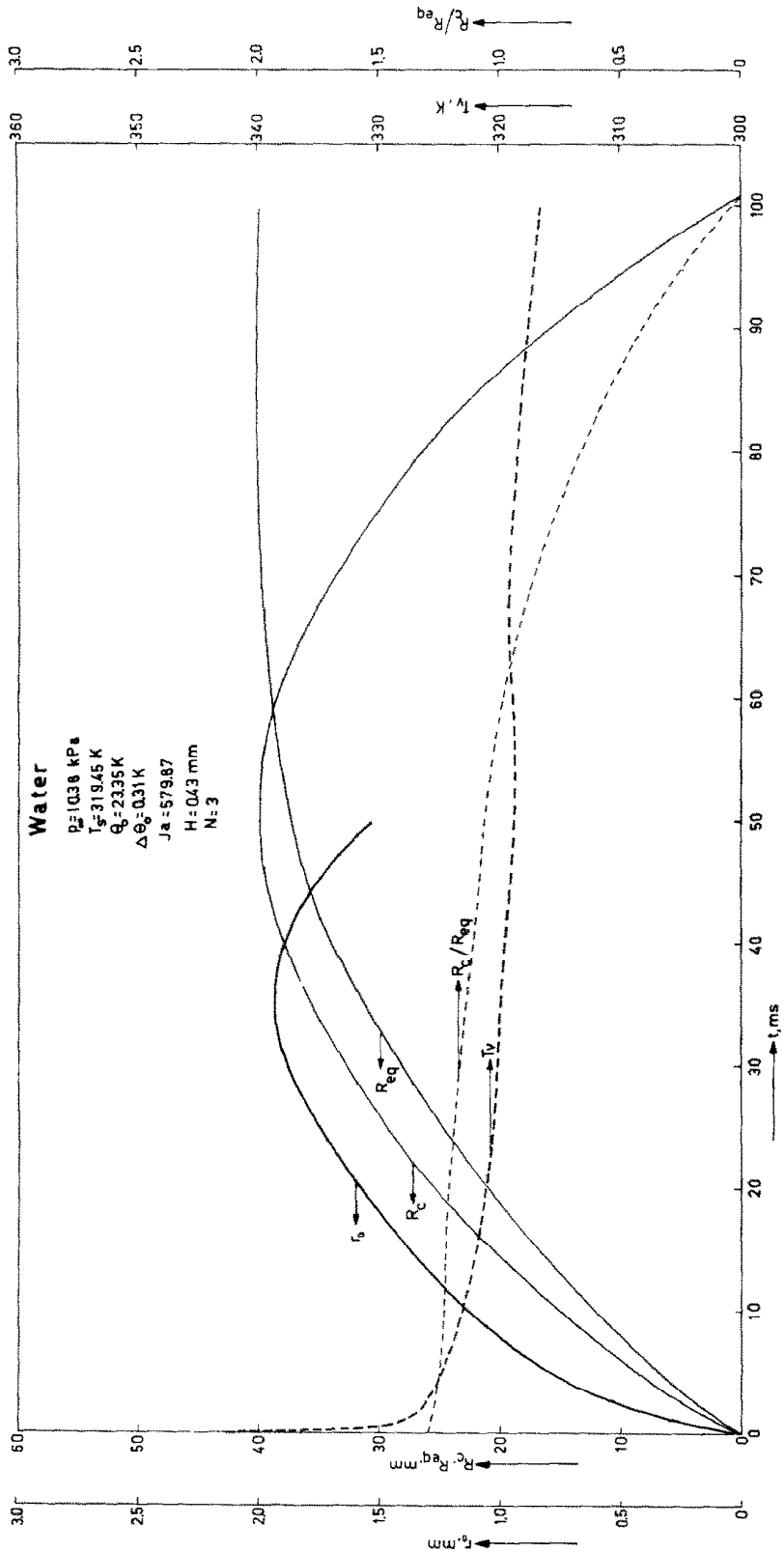

FIG. 4. Water boiling at 10.38 kPa. Numerically calculated equivalent bubble radius, R_{eq}, contact radius, R_c, ratio R_c/R_{eq}, vapour temperature, T_v and meniscus radius, r_0, in dependence on time. The height, H, of the thermal boundary layer has been fitted to corresponding experimental data, *cf.* [31].

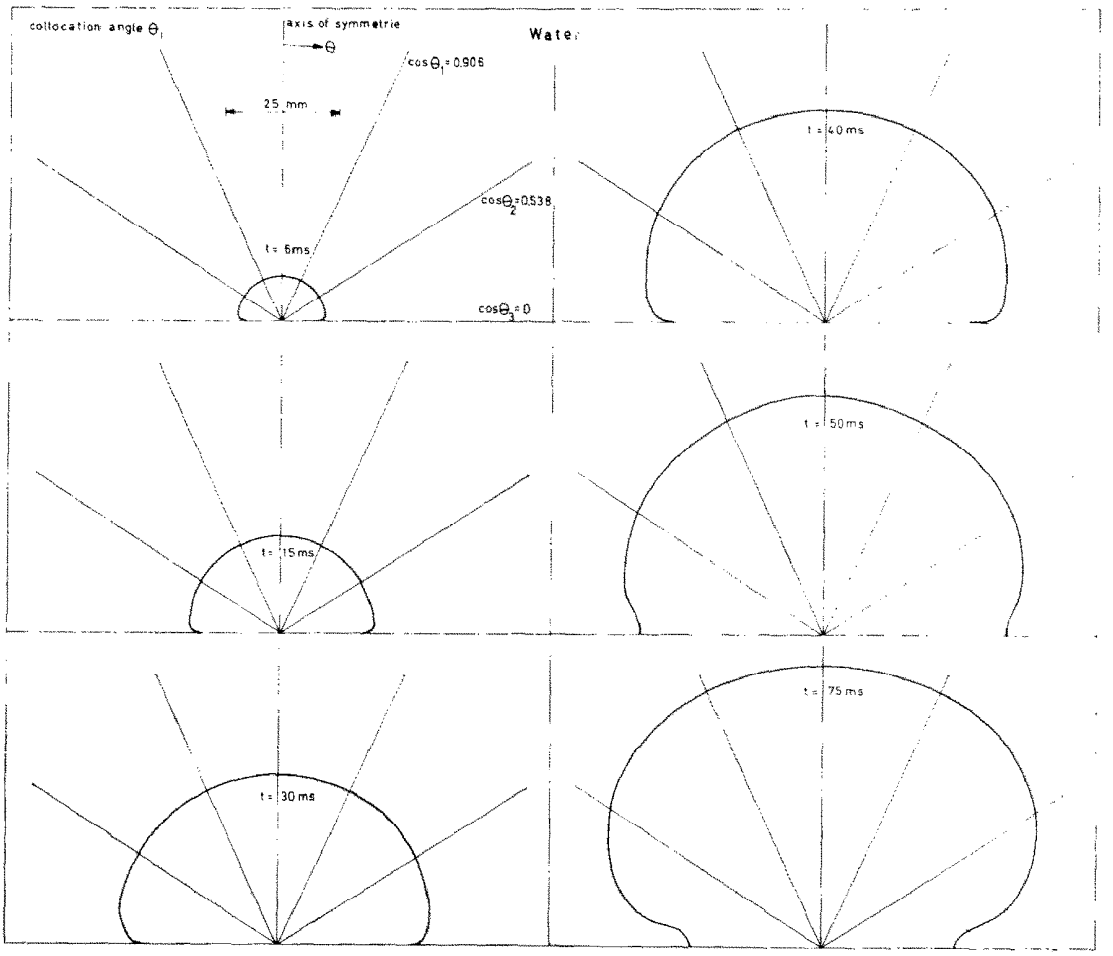

FIG. 5. Numerically calculated bubble profile in water boiling at 10.38 kPa, *cf.* Figs. 3 and 4. Initial bubble shape is hemispherical, corresponding with a small meniscus radius.

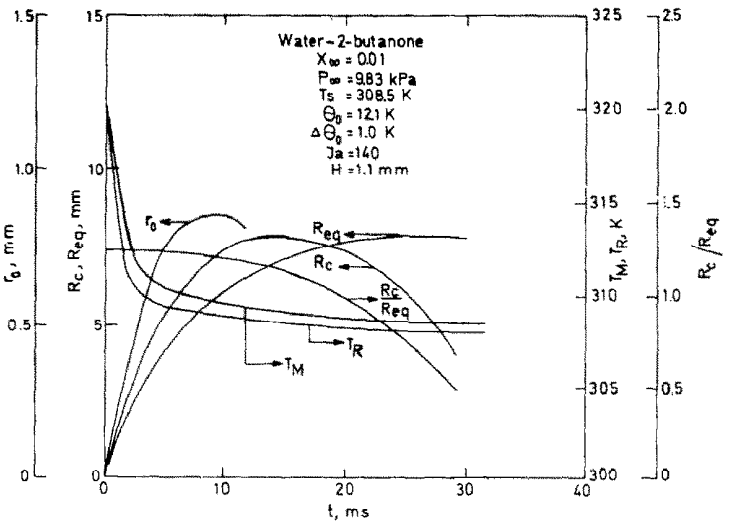

FIG. 6. Water–2-butanone, ($X_\infty = 0.01$) boiling at 9.83 kPa. Numerically calculated equivalent bubble radius, R_{eq}, contact radius, R_c, ratio, R_c/R_{eq}, vapour temperatures, T_R and T_m, and the meniscus radius r_0, in dependence on time. The vapour temperatures T_R and T_M are calculated from equations (30) and (19), respectively.

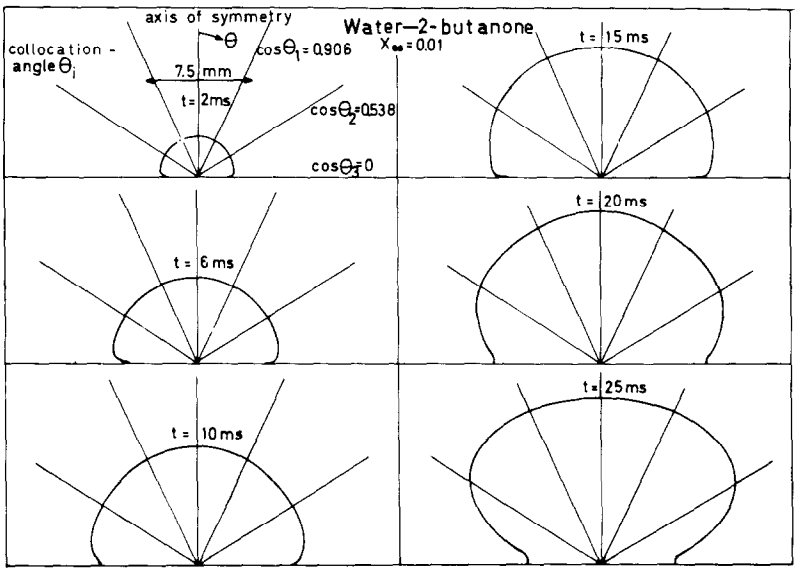

FIG. 7. Numerically calculated bubble profile in water–2-butanone ($X_\infty = 0.01$) boiling at 9.83 kPa, *cf.* Fig. 6. In comparison to water (Fig. 5), bubble growth rate is slowed down, bubble departure radius and time are decreased and the ratio of the initial meniscus radius to the bubble radius is increased.

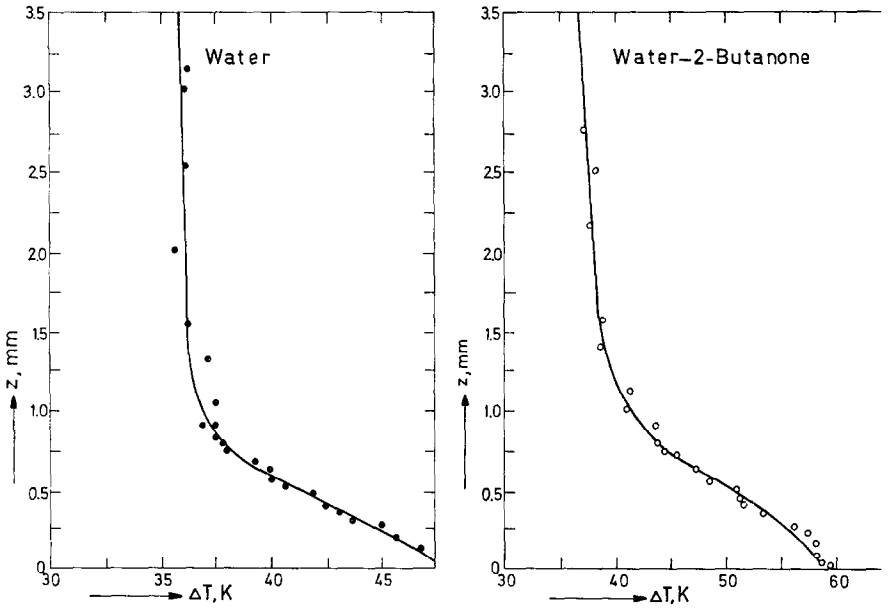

FIG. 8. Experimental temperature profile in the thermal boundary layer for water ($T_w = 321.0$ K) and for the mixture water–2-butanone ($X_\infty = 0.01$, $T_w = 331.6$ K), in absence of bubbles.

6.3. *Measurements of the initial temperature field*

In the same boiling apparatus as referred to in [30] temperature fields were measured without occurrence of a bubble, both in pure and binary mixtures.

The temperature in the thermal boundary layer has been determined by a thin thermocouple, which could be moved up and down by a micrometer. The temperature of the bulk liquid was determined by three fixed thermocouples.

The results are plotted in Fig. 8 for a pure and a binary system. The difference in thermal boundary-layer thickness between the pure and the binary system may be attributed to the fact that in the binary mixture the liquid is stirred in order to obtain a homogeneous mixture. The measured results are independent of the waiting time.

In Fig. 9 a temperature profile is measured and the saturation temperature is plotted as a function of the

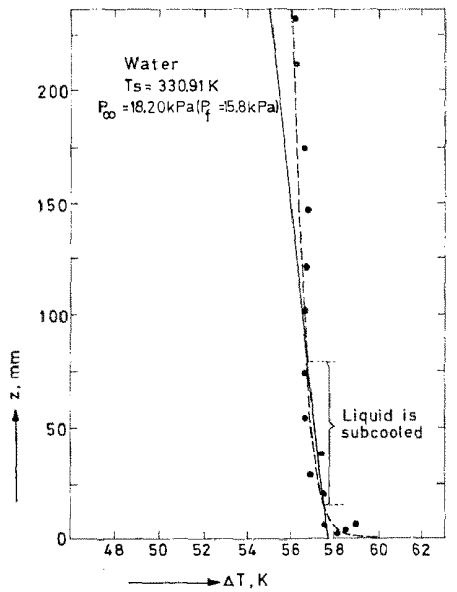

FIG. 9. Water. Experimental temperature profile (-----) and corresponding saturation temperature (——) in dependence on distance to heating surface. Locally, subcooling of liquid can occur.

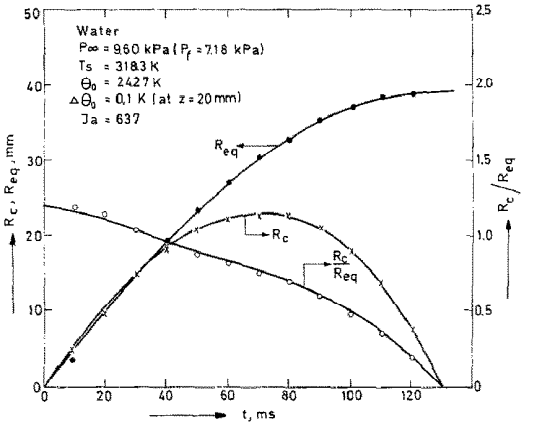

FIG. 10. Water boiling at 9.60 kPa. Experimental equivalent bubble radius, R_{eq}, contact radius, R_c, and ratio, R_c/R_{eq}, in dependence on time, *cf.* Fig. 11.

height of the liquid column. Even a region with low subcooling exists. In the numerical examples presented here, only one constant mean saturation temperature has been used.

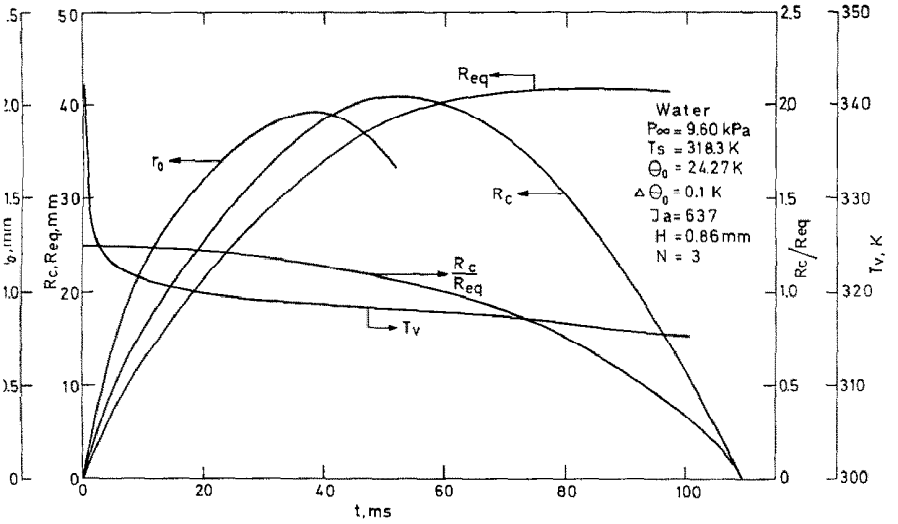

FIG. 11. Water boiling at 9.60 kPa. Numerically calculated equivalent bubble radius, R_{eq}, contact radius, R_c, ratio, R_c/R_{eq}, vapour temperature, T_v and meniscus radius, r_0, in dependence on time. The conditions are identical to Fig. 10.

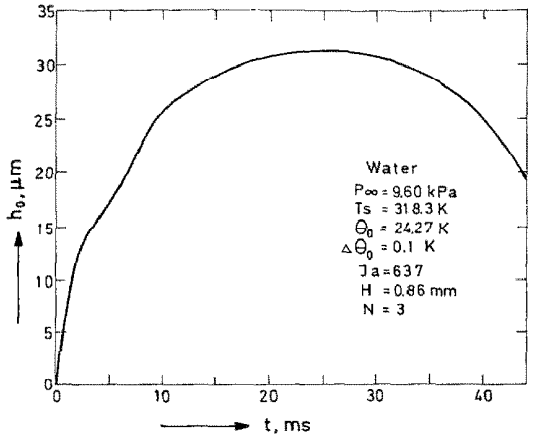

FIG. 12. Water. Theoretical initial thickness of evaporation microlayer in dependence on time for $\dot{R}_c > 0$, *cf.* Fig. 11.

6.4. *Pure water, boiling at* 9.60 kPa

Figure 10 shows the experimentally determined values of $R_{eq}(t)$ and $R_c(t)$. Figure 11 shows the computed equivalent of Fig. 10, including a plot of $r_0(t)$ for $\dot{R}_c > 0$ and of $T_v(t)$. Figure 12 presents a plot of $h_0(t)$ for $\dot{R}_c > 0$. In Fig. 13 the temperature field and bubble shape are shown for short times after bubble formation. Figure 14 shows that initially $R_c(t) \sim t$.

Figure 15 shows the hypothetical case that there would not be evaporation in the liquid microlayer. Figures 16 and 17 show the same bubble, however, growing with lower superheatings. From Figs. 15–17 it is observed that departure time and radius decrease considerably when less superheat is available.

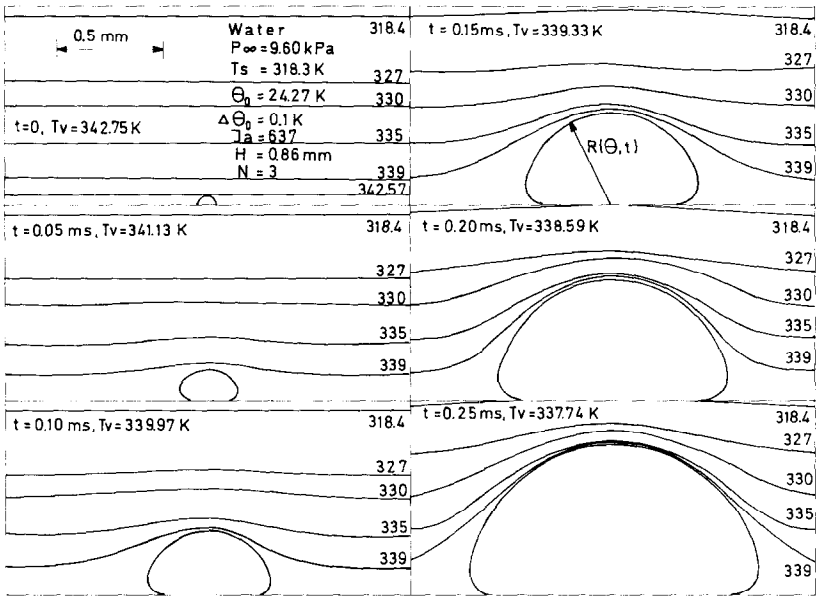

FIG. 13. Water boiling at 9.60 kPa. Numerically calculated isotherms in the liquid surrounding a growing vapour bubble.

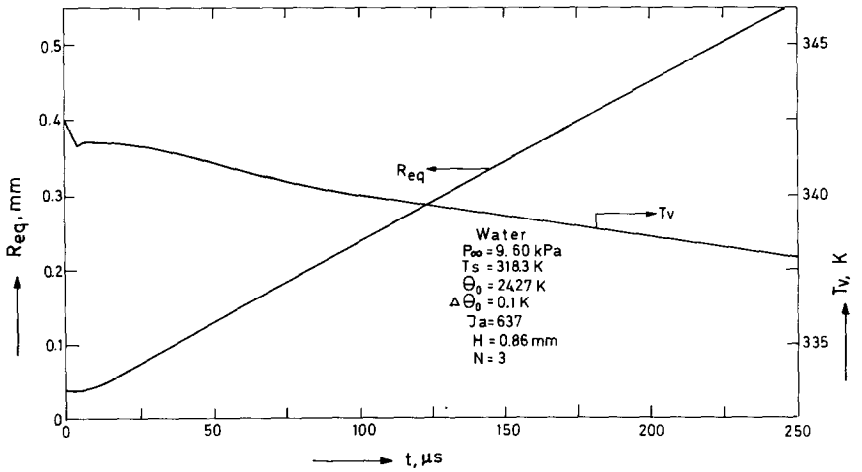

FIG. 14. Water boiling at 9.60 kPa. Numerically calculated initial equivalent bubble radius, R_{eq}, and vapour temperature T_v in dependence on time. The calculated bubble shape is hemispherical.

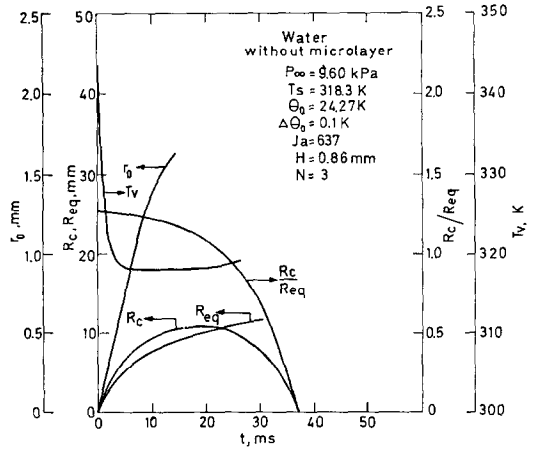

FIG. 15. Water boiling at 9.60 kPa. Numerically calculated equivalent bubble radius, R_{eq}, contact radius, R_c, ratio R_c/R_{eq}, bubble temperature T_v and meniscus radius r_0 in dependence on time. The contribution of evaporation microlayer is omitted. Cf. the results of Fig. 11, where the evaporation microlayer is taken into account.

Finally, Fig. 18 presents the same bubble under zero gravity conditions; the bubble keeps its hemispherical shape.

Acknowledgement—The authors are indebted very much to W. M. Sluyter for his valuable suggestions regarding the experimental part of this study.

REFERENCES

1. H. Bénard, Les tourbillons cellulaires dans une nappe liquide transportant de la chaleur par convection en régime permanent, *Ann. Chim. Phys.* **7**(23), 62–144 (1901).
2. Lord Rayleigh, On convection currents in a horizontal layer of fluid when the higher temperature is on the under side, *Phil. Mag.* **6**(32), 529–546 (1916).
3. P. G. Baines and A. E. Gill, On thermohaline convection with linear gradients, *J. Fluid Mech.* **37**, 289–306 (1969).
4. Y. Y. Hsu, On the size range of active nucleation cavities on a heating surface, *J. Heat Transfer* **84**(3), 207–216 (1962).
5. W. Fritz, Berechnung des Maximalvolumens von Dampfblasen, *Phys. Z.* **36**, 379–384 (1935).

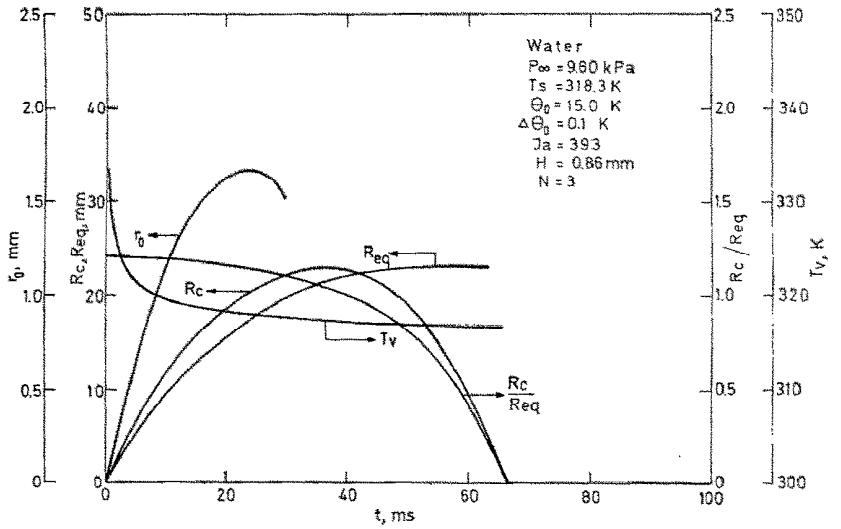

FIG. 16. Water boiling at 9.60 kPa. Numerically calculated equivalent bubble radius, R_{eq}, contact radius, R_c, ratio, R_c/R_{eq}, bubble temperature T_v and meniscus radius r_0 in dependence on time. Conditions are identical to Fig. 11, with exception of the lower wall superheating; *cf.* also Fig. 17.

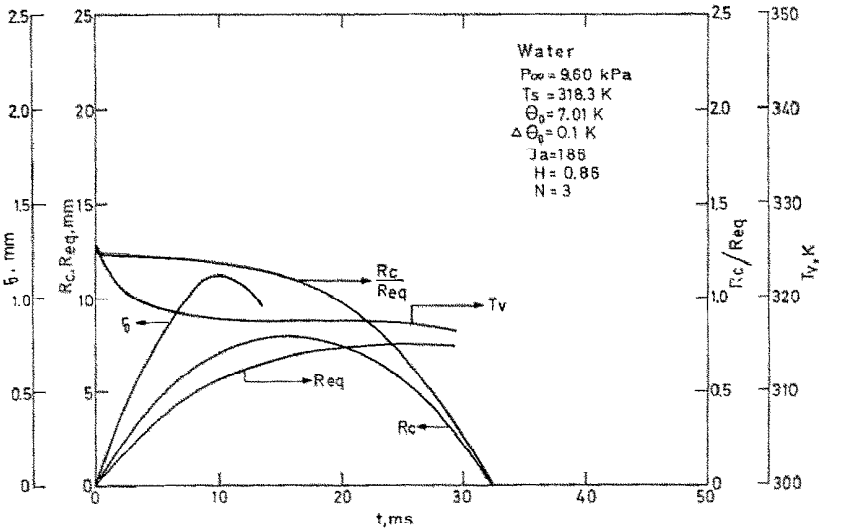

FIG. 17. Water boiling at 9.60 kPa. Numerically calculated equivalent bubble radius, R_{eq}, contact radius, R_c, ratio, R_c/R_{eq}, bubble temperature T_v, and meniscus radius r_0 in dependence on time. Conditions are identical to Figs. 11 and 16, with exception of the lower wall superheating.

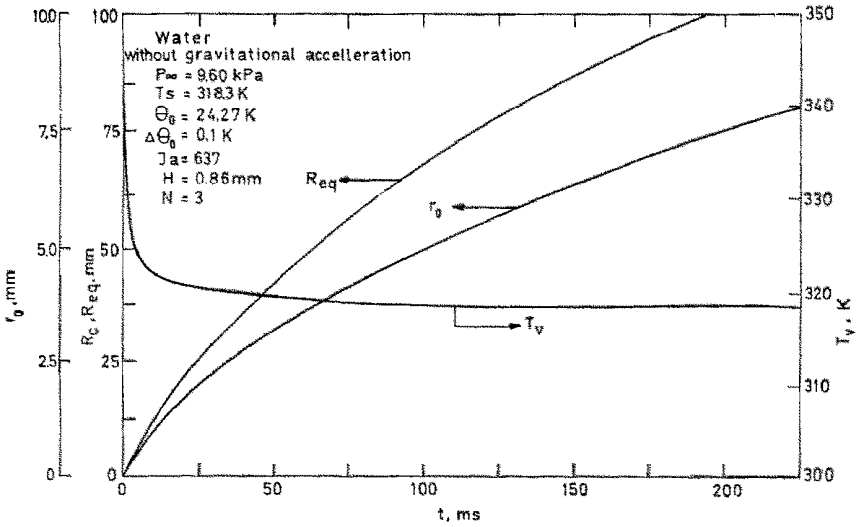

FIG. 18. Water boiling at 9.60 kPa. Numerically calculated bubble radius, R_{eq}, bubble temperature, T_v, and meniscus radius r_0 in dependence on time under zero gravity. The bubble adheres to the heating surface and remains hemispherical.

6. D. Maron-Moalem, W. Zijl and S. J. D. Van Stralen, Nucleate boiling at a liquid-liquid interface. *Letters Heat Mass Transfer* **4**, 319–329; Chapter 12 in *Boiling Phenomena*. Hemisphere, Washington, to be published.
7. F. Bošnjacović, Verdampfung und Flüssigkeitsüberhitzung, *Tech. Mech. Thermo-Dynam. Berlin.* **1**, 358–362 (1930).
8. G. Birkhoff, R. S. Margulies and W. A. Horning, Spherical bubble growth, *Physics Fluids* **1**, 201 (1958).
9. L. E. Scriven, On the dynamics of phase growth, *Chem. Engng Sci.* **10**(1), 1–13 (1959).
10. S. J. D. Van Stralen, The growth rate of vapour bubbles in superheated pure liquids and binary mixtures. Parts I and II *Int. J. Heat Mass Transfer* **11**, 1467–1489, 1491–1512 (1968).
11. W. Zijl, D. Maron-Moalem and S. J. D. Van Stralen, Inertia and diffusion controlled bubble growth and implosion in initially uniform pure and binary systems, *Letters Heat Mass Transfer* **4**, 331–339; Chapter 8 in *Boiling Phenomena*. Hemisphere, Washington, to be published (1977).
12. S. J. D. Van Stralen, Heat transfer to boiling binary liquid mixtures, *Br. Chem. Engng* **4**, 8–17 (1959); **4**, 78–82 (1959); **6**, 834–840 (1961); **7**, 90–97 (1962).
13. M. G. Cooper and A. J. P. Lloyd, The microlayer in nucleate boiling, *Int. J. Heat Mass Transfer* **12**, 895–913 (1969).
14. H. J. van Ouwerkerk, The role of the evaporating microlayer and dry surface areas in boiling, Ph.D.-Thesis, Eindhoven University of Technology (1970).
15. S. J. D. van Stralen, M. S. Sohal, R. Cole and W. M. Sluyter, Bubble growth rates in pure and binary systems: combined effect of relaxation and evaporation microlayer, *Int. J. Heat Mass Transfer* **18**, 453–467 (1975).
16. C. Y. Han and P. Griffith, The mechanism of heat transfer in nucleate pool boiling—I bubble initiation, growth and departure, *Int. J. Heat Mass Transfer*.
17. D. Maron-Moalem and W. Zijl, Growth, condensation and departure of small and large vapour bubbles in pure and binary systems. *Chem. Engng Sci.*, to be published.
18. W. Zijl, Global collocation approximations of the flow and temperature fields around a gas and a vapour bubble, *Int. J. Heat Mass Transfer* **20**, 487–498 (1977).
19. J. G. H. Joosten, W. Zijl and S. J. D. van Stralen, Growth of a vapour bubble in combined gravitational and non-uniform temperature fields, *Int. J. Heat Mass Transfer* **21**, 15–23 (1978).
20. B. Ross (editor) *Fractional Calculus and its Applications*, Lecture Notes in Mathematics. Springer, Berlin (1975).
21 K. B. Oldham and J. Spanier, *The Fractional Calculus*. Academic Press, New York (1974).
22. W. Zijl, The hydrodynamics of vapour- and gas bubbles by numerical approximation methods, in *Boiling Phenomena*, edited by S. J. D. van Stralen and R. Cole. Hemisphere Washington D.C., to be published.
23. W. Zijl, Departure of a bubble growing on a horizontal wall, Ph.D. Thesis, Eindhoven University of Technology (1978).
24. L. Landau and B. G. Levich, Dragging of a liquid by a moving plate, *Acta Phys. chim. URSS*, **17**, 1, 2, 43–54, (1942).
25. P. Groenveld, Low capillary number withdrawal, *Chem. Engng Sci.* **25**, 1259–1266, (1970).
26. R. Mesler, A mechanism supported by extensive experimental evidence to explain high heat fluxes observed during nucleate boiling, *A.I.Ch.E. Jl* **22**, 246 (1976).
27. K. B. Oldham, Diffusive transport to planar, cylindrical and spherical electrodes, *Electroanal. Chem. Interface, Electrochem.* **41**, 351–358 (1973).
28. D. B. R. Kenning and H. Toral, On the assessment of thermocapillary effects in nucleate boiling of pure fluids, presented at The Levich Birthday Conference on Physical Chemistry and Hydrodynamics, Oxford, 11–13 July (1977).
29. S. J. D. van Stralen, W. M. Sluyter and R. Cole, Bubble growth rates in nucleate boiling of aqueous binary systems at subatmospheric pressures, *Int. J. Heat Mass Transfer* **19**, 931–941 (1976).
30. H. W. Carlslaw and J. C. Jaeger, *Conduction of Heat in Solids*. Oxford University Press, London (1967).
31. S. J. D. van Stralen, R. Cole, W. M. Sluyter and M. Sohal, Bubble growth rates in nucleate boiling of water at subatmospheric pressures, *Int. J. Heat Mass Transfer* **18**, 655–669 (1975).
32. W. Zijl, The capillary induced formation of a dry area in a thin liquid layer and adherence of a growing gas bubble at a horizontal wall, ICHMT—1978 Seminar, Dubrovnik (1978).

SOLUTIONS NUMERIQUES GLOBALES DE CROISSANCE ET DE SEPARATION D'UNE BULLE SUR UNE PAROI HORIZONTALE SURCHAUFFEE DANS UN LIQUIDE PUR ET DANS UN MELANGE BINAIRE

Résumé—On étudie par des méthodes numériques globales la croissance et la séparation de bulles de vapeur sur une paroi horizontale surchauffée. La forme intégrale de l'équation de transport de la chaleur a été résolue par des développements en série obtenus par la théorie des dérivations fractionnaires. La méthode de colocation orthogonale est appliquée à l'écoulement potentiel autour de la bulle. De cette manière un système de huit ou dix équations différentielles est intégré par ordinateur. Les résultats, pour des répartitions données de température initiale sont en accord quantitatif avec des résultats experimentaux obtenus dans l'eau et des mélanges binaires aqueux en ébullition à la pression atmosphérique.

GLOBALE NUMERISCHE LÖSUNG FÜR WACHSTUM UND ABLÖSUNG EINER DAMPFBLASE AN EINER HORIZONTALEN ÜBERHITZTEN WAND IN EINER REINEN FLÜSSIGKEIT UND EINEM BINÄREN GEMISCH

Zusammenfassung—Das Wachstum und das durch Auftrieb hervorgerufene Ablösen von Dampfblasen an einer horizontalen überhitzten Wand wurden mittels globaler numerischer Methoden untersucht. Die Integralformen der Wärmetransportgleichung wurden mit Hilfe von Reihenentwicklungen gelöst, die man aus der Theorie der partiellen Ableitungen erhalten hatte. Für die Potentialströmung um die Blase wurde die globale orthogonale Kollokationsmethode angewandt. Auf diese Art und Weise ist nur ein Satz von acht oder zehn einfachen Differentialgleichungen vom Computer zu integrieren. Die Ergebnisse, die sich aus vorgegebenen Anfangstemperaturverteilungen ergeben, stimmen quantitativ mit experimentellen Daten überein, die durch Siedeversuche bei unteratmosphärischen Drücken mit Wasser und wäßrigen binären Gemischen gewonnen wurden.

ОБОБЩЕННОЕ ЧИСЛЕННОЕ ИССЛЕДОВАНИЕ РОСТА И ОТРЫВА ПАРОВЫХ ПУЗЫРЬКОВ НА ГОРИЗОНТАЛЬНОЙ ПЕРЕГРЕТОЙ СТЕНКЕ В ЧИСТОЙ ЖИДКОСТИ И БИНАРНОЙ СМЕСИ

Аннотация — С помощью обобщённых численных методов исследуется рост и вызванный плавучестью отрыв паровых пузырьков на горизонтальной перегретой стенке. Интегральные уравнения переноса тепла решены с помощью разложений в ряды в рамках теории дробных производных. Для описания потенциального обтекания пузырьков использовался обобщенный ортогональный метод коллокаций, что позволило проинтегрировать на компьютере систему только из восьми или десяти обыкновенных дифференциальных уравнений. При заданных начальных распределениях температуры полученные результаты количественно согласуются с экспериментальными данными для воды и водных бинарных смесей, кипящих при давлениях, ниже атмосферного.